Chem Soc Rev

A Historical Overview of the Activation and Porosity of Metal–Organic Frameworks

Journal:	*Chemical Society Reviews*
Manuscript ID	CS-REV-08-2020-000997.R1
Article Type:	Review Article
Date Submitted by the Author:	02-Sep-2020
Complete List of Authors:	Zhang, Xuan; Northwestern University, Chen, Zhijie; Northwestern University, Department of Chemistry Liu, Xinyao; Jilin University, College of Chemistry Hanna, Sylvia; Northwestern University, Chemistry Wang, Xingjie; Northwestern University, Chemistry Taheri-Ledari, Reza; Catalysts and Organic Synthesis Research Laboratory, Department of Chemistry, Iran University of Science and Technology, Tehran 16846-13114, Iran, Chemistry Maleki, Ali; Iran University of Science and Technology, Department of Chemistry Li, Peng; Fudan University, Chemistry Farha, Omar; Northwestern University, Department of Chemistry

ARTICLE

A Historical Overview of the Activation and Porosity of Metal–Organic Frameworks

Received 00th January 20xx,
Accepted 00th January 20xx

DOI: 10.1039/x0xx00000x

Xuan Zhang,[a] Zhijie Chen,[a] Xinyao Liu,[a,d] Sylvia L. Hanna,[a] Xingjie Wang,[a] Reza Taheri-Ledari,[c] Ali Maleki,[c] Peng Li,[e] Omar K. Farha *[a,b]

Since the first reports of metal–organic frameworks (MOFs) , this unique class of crystalline, porous materials has garnered increasing attention in a wide variety of applications such as gas storage and separation, catalysis, enzyme immobilization, drug delivery, water capture, and sensing. A fundamental feature of MOFs is their porosity which provides space on the micro- and meso-scale for confining and exposing their functionalities. Therefore, designing MOFs with high porosity and developing suitable activation methods for preserving and accessing their pore space have been a common theme in MOF research. Reticular chemistry allows for the facile design of MOFs from highly tunable metal nodes and organic linkers in order to realize different pore structures, topologies, and functionalities. With the hope of shedding light on future research endeavors in MOF porosity, it is worthwhile to examine the development of MOFs, with an emphasis on their porosity and how to properly access their pore space.. In this review, we will provide an overview of the historic evolution of porosity and activation of MOFs, followed by a synopsis of the strategies to design and preserve permanent porosity in MOFs.

1. Introduction

The development of porous materials has been essential for technologies in various aspects of everyday life and industrial applications, such as bath sponges, filters, masks, foams, adsorbents and catalysts. One major feature of porous materials is their low density, as they contain a large fraction of void space, within which countless functionalities can be designed based on the desired applications. Crystalline porous materials, which have long-ranged ordered structures, have been of particular interest due to the diverse and facile control of their structures and properties.[1]

Even though synthetic zeolites—comprised of solely inorganic components such as silicates and aluminates—have been extensively studied since the 1940s, it was not until the late 1980s and early 1990s that the first crystalline porous materials with pore sizes of larger than 1 and 2 nm were reported, respectively.[2,3] In 1995, a unique class of crystalline porous materials, termed metal–organic frameworks (MOFs) by Yaghi,[4,5] emerged and has since distinguished itself with permanent porosity and high surface areas, due to the strong bonds between metal ions and charged organic ligands.[6] The highly tunable inorganic and organic building units of MOFs have opened up a new chapter in the design and applications of porous materials. In addition to the various possible combinations of inorganic and organic building units with different geometries and functionalities, MOFs offer unparalleled adaptability in isoreticular manipulation;[7] while keeping the structural design and topology invariant, a vast number of alterations in their structures and functionalities can be readily accessed during synthesis or *via* post-synthetic modifications. The conception and development of reticular chemistry has been monumental for the synthesis and application of porous crystalline framework materials like MOFs.[8] Over the past few decades, over 100,000 structures have been reported in the "MOF subset"[9-11] of the Cambridge

[a] *Department of Chemistry and International Institute for Nanotechnology, Northwestern University, Evanston, Illinois 60208, United States.*
[b] *Department of Chemical and Biological Engineering, Northwestern University, 2145 Sheridan Road, Evanston, Illinois 60208, United States.*
[c] *Department of Chemistry, Iran University of Science and Technology, Tehran 16846-13114, Iran.*
[d] *State Key Laboratory of Inorganic Synthesis and Preparative Chemistry, College of Chemistry, Jilin University, Changchun 130012, P. R. China.*
[e] *Department of Chemistry and Shanghai Key Laboratory of Molecular Catalysis and Innovative Materials, Fudan University*

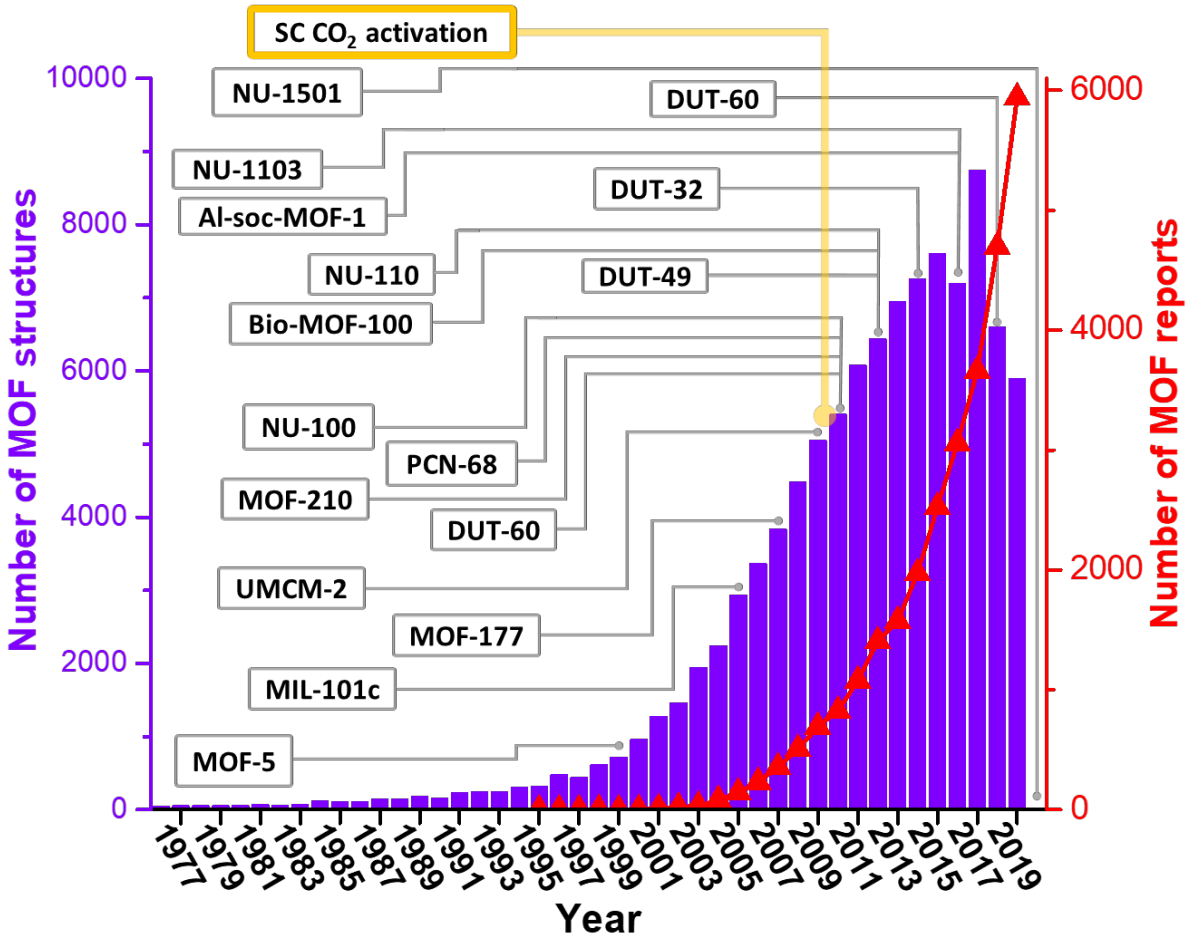

Figure 1. Number of MOF structures in the Cambridge Structural Database (CSD) and MOF reports found in Web of Science, from 1976 to 2019. The structural data was summarized from the MOF subset of CSD as of May 2020. Numerous representative high porosity MOFs are indicated in the plot according to the year they were reported. The first use of supercritical CO_2 drying for activating MOFs is indicated in yellow.

Structural Database (CSD), and the number of MOF-related research publications has been continuously increasing (Figure 1).

One of the most notable characteristics of MOFs is their high porosity, which has made their implementation in gas storage,[7,12] small-molecule separations,[13-15] catalysis,[16-19] sensing,[20,21] biomolecule encapsulation,[22-24] drug delivery,[25,26] conductivity,[27,28] magnetism,[29-31] and other applications possible. Even though the primitive concept of porosity in metal–organic materials with extended structures was conceived in the late 1980s and early 1990s,[5,32,33] it was not until the late 1990s that the first experimental gas adsorption measurements of these inorganic–organic hybrid materials were reported.[6,34] Kitagawa reported room temperature gas adsorption isotherms at high pressures and showed that metal–organic polymers were able to take up gas phase guest molecules.[34] In 1998, Yaghi reported the first MOF showing permanent porosity with nitrogen adsorption/desorption isotherms at 77 K and low pressure (Figure 2)—a procedure that has been employed before for probing permanent porosity in other porous materials such as zeolites, porous silica, and porous carbon—and derived the first values of apparent surface area and pore volume in a MOF.[6] Compared to previous works where only guest exchange/removal had been observed to

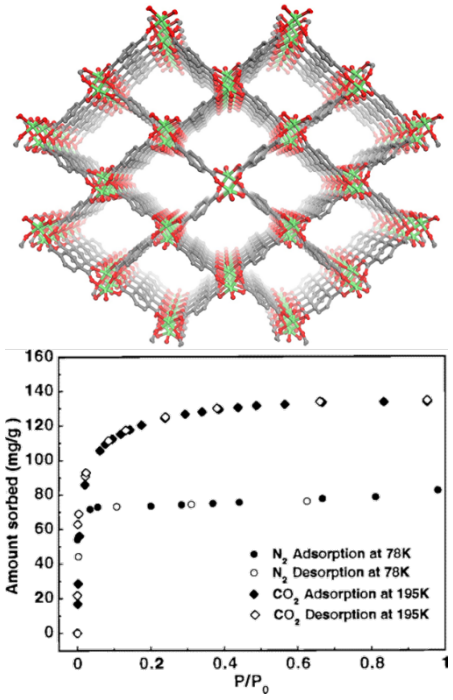

Figure 2. The crystal structure (top) and the gas adsorption/desorption isotherms for the MOF Zn(BDC) showing permanent porosity. Adapted with permission from ref. 6. Copyright 1998, American Chemical Society.

support the presence of porosity in MOFs, these gas adsorption measurements of MOFs in the de-solvated state marked a milestone in the development of porous MOFs and laid the foundation of achieving permanent porosity in MOFs.[34]

The prosperity of MOFs as high surface area materials has since blossomed. The underlying principles of reticular chemistry, as established by Yaghi, have guided the design and development of MOFs.[35-40] Not only do the design and synthesis of MOFs play an important role in achieving higher porosity and stability in MOFs, but the development of improved activation methods is also essential in enabling the access to their porosity.[41,42] For instance, it has often been found that a MOF's Brunauer-Emmett-Teller (BET) area can be significantly increased with a better developed activation method, especially for MOFs with exceptionally high porosity where mild activation conditions like supercritical CO_2 drying are required (Table 1 and Figure 3).[43-45]

To this date, MOFs have garnered tremendous attention from different areas of research not only for the purpose of designing and synthesizing new materials, but also for a wide variety of applications. Based on the foundation of reticular chemistry, an enormous library of empirical and theoretical protocols for designing MOFs with tailored pore structures and functionalities has been established.[8,63] The field of MOF chemistry cannot be where it is today without all the researchers' continuous passion, creativity and hard work. Therefore, it is worthwhile to examine the evolution of MOFs, with an emphasis on their porosity and how to properly access their porosity from a historical point of view. In this review, we provide an overview of the development of MOF porosity and activation, followed by a synopsis of the strategies to design and preserve MOF permanent porosity.

Materials	Year reported	BET area ($m^2\ g^{-1}$)[a]	Pore volume ($cm^3\ g^{-1}$)[a]	Topology	Activation method[d]	Ref.
MOF-5	1999, 2007	3800	1.55	**pcu**	Thermal	43,46
MIL-101c	2005, 2008	4230	2.15	**mtn-e**	Chemical and Thermal	44,47
bio-MOF-100	2012	4300	4.3	**lcs-a**	Supercritical CO_2	48
MOF-205/DUT-6	2009, 2010	4460	2.16	**ith-d**	thermal	49,50
MOF-177	2007	4750	1.89	**qom**	thermal	51
MOF-200	2010	4530	3.59	**qom**	Supercritical CO_2	50
PCN-68	2010	5110	2.13	**rht**	Thermal	52
UMCM-2	2009	5200	2.32	**umt**	Room temperature vacuum	53
DUT-49	2012	5480	2.91	**nbo**	Supercritical CO_2	54
Al-soc-MOF-1	2015	5590	2.3	**soc**	Thermal	55
NU-100	2010	6140	2.82	**rht**	Supercritical CO_2	56
MOF-210	2010	6240	3.60	**toz**	Supercritical CO_2	50
DUT-76	2015	6340	3.25	**ftw**	Supercritical CO_2	57
DUT-32	2014	6410	3.16	**umt**	Supercritical CO_2	58
NU-1103	2015	6550	2.91	**ftw**	Supercritical CO_2	59
NU-110	2012	7140	4.40	**rht**	Supercritical CO_2	60
NU-1501-Al[b]	2020	7310	2.91	**acs**	Supercritical CO_2	61
DUT-60[c]	2018	7840	5.02	**ith-d**	Supercritical CO_2	62
NU-1501-Al[c]	2020	9140	2.91	**acs**	Supercritical CO_2	61

Table 1. A list of selected highly porous MOFs.

[a] BET area and experimental pore volume are obtained from the reported values or N_2 adsorption isotherm in the reported literature. [b] BET area calculated after satisfying all four BET consistency criteria. [c] BET area calculated after satisfying first two BET consistency criteria. [d] Thermal activation conventionally refers to heating under dynamic vacuum above room temperature.

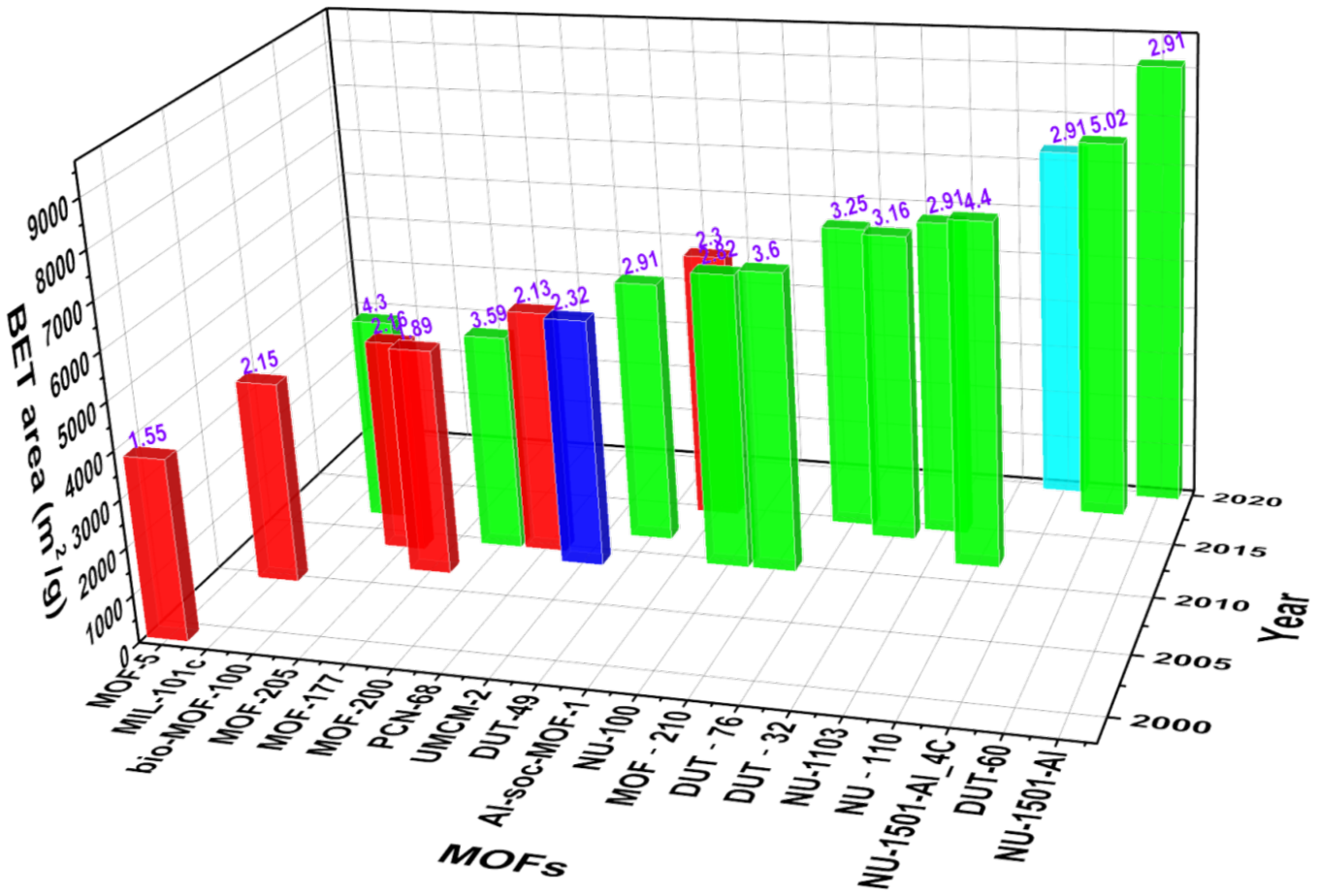

Figure 3. The development trend of representative highly porous MOFs according to the year they were reported and their BET area. The data is color-coded according to their activation methods and BET area calculation criteria. The pore volumes (cm^3/g) are labelled in purple on the corresponding bars.

2. Porosity and MOFs

2.1 Classification and adsorptive measurements

According to recommendations by the International Union of Pure and Applied Chemistry (IUPAC), porous materials such as activated carbon, zeolites and MOFs are classified into three categories—microporous, mesoporous, and macroporous—based on pore sizes.[64-66] Microporous materials have a pore width of smaller than 2 nm, mesoporous materials have pore sizes between 2 nm and 50 nm, and macroporous materials contain pores greater than 50 nm. Generally, researchers collect adsorption isotherms using probe molecules such as nitrogen (N_2) and argon (Ar) at their standard boiling points to study the porosity of MOFs. For example, a nitrogen adsorption isotherm is collected at 77 K while an argon isotherm is collected at 87 K (boiling points of the adsorbates). IUPAC recommends using Ar (87 K) adsorption for materials with polar functionalities, since the nitrogen molecule can interact with functional surfaces due to its quadrupole moment. However, most research groups use N_2 adsorption experiments to study the porosity of MOF materials because it is highly accessible and inexpensive. Although IUPAC recommends avoiding carbon dioxide (CO_2) to analyze porous materials with polar surfaces due to the even stronger quadrupole moment of CO_2 compared to N_2, CO_2 adsorption is sometimes applied to access the porosity of MOFs with small pore sizes (e.g. smaller than 0.45 nm) when N_2 and Ar molecules are hard to diffuse into the pore space of MOFs.[67]

Typically, adsorption data are presented in the format of "quantity of gas adsorbed" plotted against "relative pressure", and called a physisorption isotherm. IUPAC categorized[65,66] physisorption isotherms into six classic types (i.e. from type I to type VI). Most physisorption isotherms of rigid MOFs are based on type I (microporous) and type IV (mesoporous), while many isotherms of flexible MOFs[68-74] display shapes different from the six representative types. The structural transformation of flexible MOFs over the course of the adsorption process makes their isotherms very difficult to be interpreted. Therefore, there is a pressing need to further develop novel approaches to analyze and classify new types of physisorption isotherms observed in flexible MOFs.[75] It is worth mentioning that adsorption of other adsorbates such as water often display other types of isotherms and the shape of the isotherm can be dependent on the intricate properties of the MOF adsorbents.[76-79]

2.2 Surface area, pore volume and pore size distribution

After the establishment of permanent porosity in MOFs,[6] collecting physisorption isotherms has become a routine

method to characterize MOF materials. The interpretation of a physisorption isotherm such as a nitrogen or argon adsorption isotherm provides information such as surface area, pore volume and pore size distribution.

Based on a multilayer adsorption model, the Brunauer-Emmett-Teller (BET) method[80] is commonly applied to evaluate the surface area of porous MOFs.[81,82] The BET equation is applicable for many Type II and Type IV isotherms for porous materials with pore width greater than 4 nm. However, it is suggested by IUPAC to apply the BET method with high caution when micropores are present, which is the case for most MOFs.[66] It is problematic to differentiate monolayer adsorption, multilayer adsorption, and micropore filling in the case of MOFs containing micropores, and this leads to the difficulty of locating a linear range for BET calculations. To that end, "apparent BET surface area" or "estimated BET area" is a recommended term to be widely used. Strict criteria such as the four BET consistency criteria proposed by Rouquerol *et al*.[82] should be applied to determine the linear range for calculating the estimated BET area.

$$\frac{P/P_0}{N(1-P/P_0)} = \frac{1}{N_m C} + \frac{C-1}{N_m C}\left(\frac{P}{P_0}\right)$$

In the equation above, the first criterion is to select a range with $N(1-P/P_0)$ increasing monotonically with P/P_0, where N denotes the adsorbate loading and P/P_0 denotes relative pressure. Second, the value of C from the linear regression needs to be positive. Third, a relative pressure P/P_0 related to N_m, the monolayer loading, should fall within the selected linear region. Fourth, the P/P_0 related to the monolayer loading determined based on BET theory (i.e. $1/\sqrt{C}$ + 1) should be close to the relative pressure calculated in the third criterion. For the last criterion, a tolerance of 20% is recommended by Rouquerol et al.[81,83]

Practically, when it is impossible to select a region from experimental isotherms to fulfill all four BET consistency criteria, the deviation from these criteria is recommended to be minimized.[83] It is important to note that many reported values of BET area fulfill only the first two BET consistency criteria, but we believe the use of all four BET consistency criteria is projected to be the trend, particularly for highly porous MOFs with high surface areas.[61,83,84] Despite its limitations, BET area provides a well-accepted comparison of surface area for MOFs and can be used as a valuable fingerprint of MOF adsorbents.

Pore volume is another vital parameter for assessing the porosity of MOFs. Ideally, if a MOF has minimal external surface area and does not contain large pores such as macropores, a virtually horizontal plateau is expected to be observed. Type I isotherms for a microporous MOF and Type IV isotherm for a mesoporous MOF reach the plateau of the adsorption isotherm when it is saturated with adsorbed molecules. By applying the Gurvich rule[65,85,86], assuming that the pores of MOFs are filled with the condensed adsorbate in the liquid state, the experimental pore volume can be calculated from the adsorbed capacity. Total pore volume is typically derived from uptake at a relative pressure approaching unity. On the other hand, the theoretical pore volume of MOFs can be calculated from a crystal structure and serves as a good reference for the experimental pore volume.[87]

When interpreting the pore size distribution from isotherms, both pore geometries (e.g. slit, cylinder, and spherical) and kernels should be considered. Pore size distributions calculated from MOF isotherms, distributing total pore volume into the different pore widths, can vary significantly depending on the selected shape models and kernels. Several methods such as Horvath-Kawazoe (HK), density functional theory (DFT), and Monte Carlo simulation (MC) have been developed over the years for deriving pore size distribution.[81,88,89] The DFT pore size distribution, despite theoretical limitations assuming a molecularly smooth surface, offers a reasonably accurate evaluation for most porous MOFs. To this end, it is important to

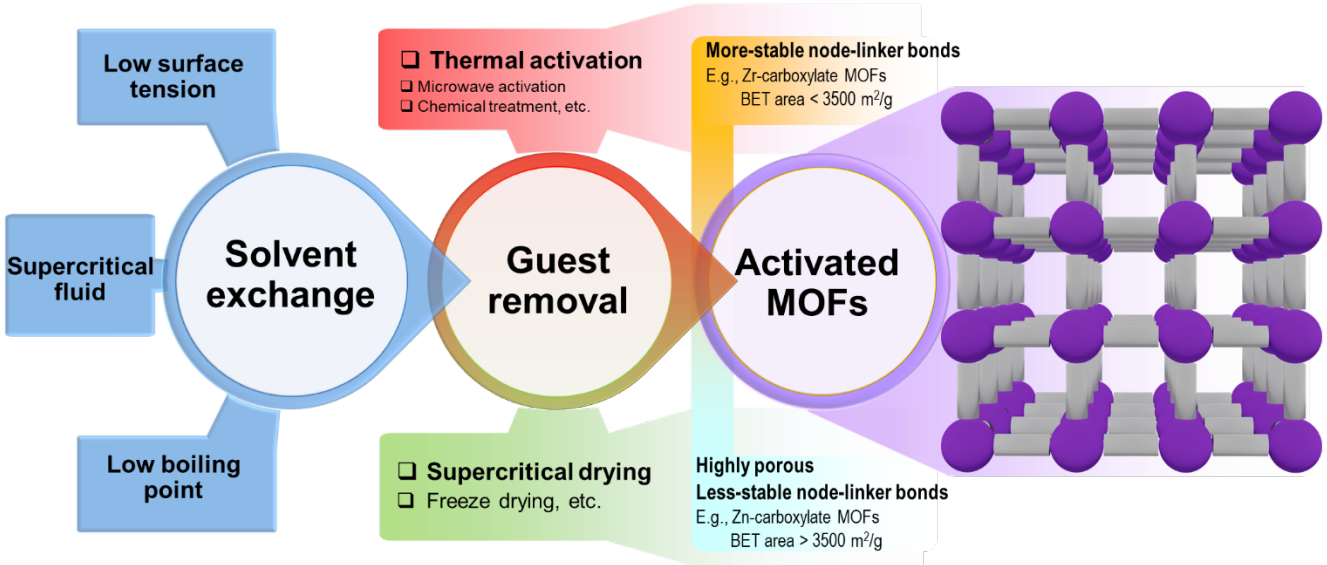

Scheme 1. Overview of the workflow and strategies of MOF activation. As an empirical guideline, thermal, microwave and chemical activation are viable for MOFs with more-stable node-linker bonds such as Zr-carboxylate-based MOFs, and MOFs with BET area smaller than 3500 m^2/g; supercritical and freeze drying are likely needed for MOFs with less-stable node-linker bonds such as Zn-carboxylate MOFs, or highly porous MOFs with BET area larger than 3500 m^2/g.

develop better pore size distribution models for MOFs, particularly flexible MOFs.

3. Development of Strategies for the Activation of MOFs

Understanding the intrinsic physical properties of MOFs is critical for their applications. Due to the fact that as-synthesized MOFs usually contain guest molecules (such as solvents, unreacted linkers, clusters, and modulators), it is usually necessary to remove these guest species through an activation process to access the pore space of MOFs for their applications (Scheme 1). Since different guest molecules interact with the host framework with varying strength, suitable and thorough activation methods that avoid compromising the structural integrity of the MOFs are critical to realizing the maximum surface area and pore volume, especially for MOFs with relatively weak node-linker bonding or large pores. In this section, a few common activation techniques will be highlighted, and some remaining challenges will be discussed. It is noted that in many cases, there is no clear-cut boundary of the optimal activation strategies, and a combination of activation methods may be necessary to achieve the desired results for a particular MOF.

3.1 Thermal activation

Since the majority of MOFs are synthesized in solvent, especially high boiling point solvent like *N, N*-dimethylformamide (DMF), *N, N*-diethylformamide (DEF), and dimethyl sulfoxide (DMSO), vacuum evacuation at elevated temperatures after exchanging with low boiling point solvents, such as acetone, methanol and dichloromethane, is a routine way to activate MOFs. This process has been widely utilized for traditional porous materials such as porous carbon and zeolites and is known as "thermal activation", even though pre-treatment of as-synthesized MOFs by solvent-exchange and the use of vacuum are additionally required. While certain types of MOFs suffer from low stability (*vide infra*), more and more MOFs with high thermal and chemical stability have been reported, allowing them to be directly activated by conventional thermal activation. For example, Cr- and Zr-carboxylate-based MOFs such as Cr-MIL-101 ($Cr_3F(H_2O)_2O[(O_2C)\text{-}C_6H_4\text{-}(CO_2)]_3$)[90] and UiO-66 ($Zr_6(O)_4(OH)_4(bdc)_{12}$)[91] have been well-known for their high thermal and chemical stability due to their strong Cr-O/Zr-O bonds. These samples can be activated by conventional thermal activation to remove the remaining water and DMF solvents in the pores, respectively. The surface area for these two materials thus can reach 4100 $m^2\ g^{-1}$ and 1100 $m^2\ g^{-1}$, respectively. Therefore, given the strong M-O bonds, one can consider this method as a choice if not pursuing the highest BET surface area and pore volume.[92,93] For MOFs that were synthesized with low boiling point solvents (e.g. ethanol and acetonitrile), one can also find this method worth attempting. However, most MOFs are crystallized in one or a combination of multiple high boiling point solvents including DMF, DMSO, H_2O, DEF, and acid. Without strong M-O bonds and high thermal stability, the structure of these MOFs will collapse to some extent if activated thermally. This can be ascribed to the high surface tension and capillary forces, which were generated during the liquid-to-gas phase transformation of the guest solvents during the activation process.

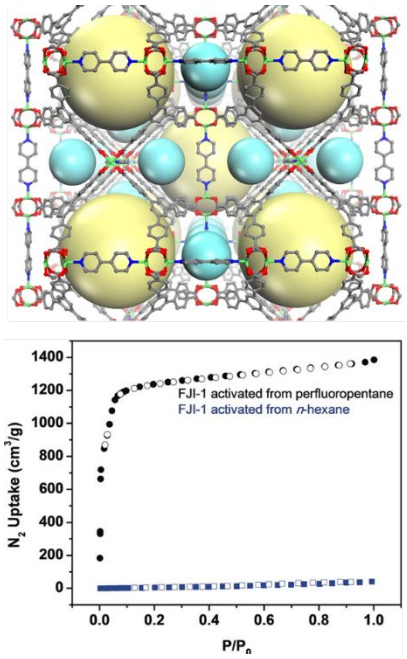

Figure 4. N_2 isotherm plots of FJI-1 activated from perfluoropentane and n-hexane exchanged materials. Inset: structure of FJI-1. Adapted with permission from ref. 109. Copyright 2017, Wiley-VCH Verlag GmbH & Co. KGaA, Weinheim.

Table 2. Surface tension (20 ˚C) and boiling points of selected solvents.

Solvents	Surface tension /mN·m^{-1}	Boiling point /˚C
Perfluopentane	9.42	28
Perfluohexane	11.91	56
Perfluooctane	14	133
Pentane	15.48	36.1
diethyl ether	17.06	34.6
n-Hexane	18.43	69
2,2,3-trimethyl butane	18.99	80.8
Acetonitrile	19.1	82
Tert-butylchloride	19.6	51
n-Heptane	20.14	98.4
n-Octane	21.6	125.5
Ethanol	22	78.4
Methanol	22.1	64.7
Acetone	23	56.5
Tetrahydrofuran	26.4(25 ˚C)	66
Dichloromethane	27.8	39
Chloroform	27.1	61.2
DMF	34.4	153
DMSO	42.9	189

Water	72.7	100

A modified method was then developed to lower the capillary forces of solvent evaporation during the MOF activation. Exchanging the high boiling point and/or high surface tension solvents with low boiling point and/or low surface tension solvents before the heat/vacuum treatment is now the most commonly used method in MOF activation. As listed in Table 2, common lab solvents like methanol, acetone, ethanol, diethyl ether, and acetonitrile possess lower surface tension and boiling points compared to DMF, DMSO, and H_2O. In general, solvent-exchange to these low boiling-point solvents should suffice for the activation of most MOFs.[94-107] However, in some cases where these common solvents still fail to obtain the expected surface area and pore volume, one could consider turning to solvents with much lower surface tension, such as pentane and fluorocarbons to complete the solvent exchange. For example, due to lack of thermal stability above 120 ˚C for Yb-NH_2-TPDC (H_2-NH_2-TPDC = 3,3''-diamino-1,1':4',1''-terphenyl-4,4''-dicarboxylic acid), Rosi and coworkers reported that by stepwise solvent exchange with dichloromethane and n-pentane(15.48 $mN{\cdot}m^{-1}$), the MOF could be activated under vacuum at room temperature to achieve a BET area of 2370 m^2/g.[108] Metzger and coworkers also showed that SNU-70 and UMCM-9 exhibited rather low surface areas if THF (26.4 $mN{\cdot}m^{-1}$) and CH_2Cl_2(27.8 $mN{\cdot}m^{-1}$) were used as the exchanging solvents, while much higher BET areas of 5300 and 5170 $m^2{\cdot}g^{-1}$, respectively, were achieved by exchanging with n-hexane, a solvent with much lower surface tension.[109] They also observed that FJI-1, a Zn paddle-wheel ($Zn_2(CO_2R)_4$)-based fragile MOF, only exhibited a BET area of ~100 $m^2{\cdot}g^{-1}$ when n-hexane was used. When a lower surface tension solvent, perfluoropentane (9.42 $mN{\cdot}m^{-1}$), was used for the solvent exchange with subsequent evacuation at room temperature, the activated material then reached a high BET area of 4890 $m^2{\cdot}g^{-1}$ (Figure 4), similar to the theoretical surface area value of 4740 $m^2{\cdot}g^{-1}$.[109] These results suggest that solvent exchange with low surface tension solvents can facilitate the full activation of MOFs. However, one may notice that n-hexane and diethyl ether might be the lowest surface tension solvents commonly found, while fluorocarbons are less commonly used and are more costly (the price for perfluoropentane is about 200 times higher than that of acetone). As a result, an alternative mild activation process that is more cost-effective is desirable.

3.2 Supercritical CO_2 drying

Following the logic of using lower surface tension solvents for the activation of MOFs under milder conditions, a supercritical fluid, possessing no surface tension, was deemed desirable for this purpose. Supercritical CO_2 (sc-CO_2) is a safe, non-flammable, and inexpensive resource that has been employed in processes of supercritical extraction (e.g. decaffeination of coffee) and lyophilization of delicate structures (e.g. biological specimens and aerogels).[110] Similar to the conventional activation process, sc-CO_2 drying involves three general steps: pre-exchanging the as-synthesized solvents with liquid CO_2 compatible organic solvents, exchanging the organic solvents with liquid CO_2, and evaporating off CO_2 in its supercritical state. Before sc-CO_2 activation, the solvents of an as-synthesized MOF sample are exchanged with a solvent that can be miscible with liquid CO_2 and will not cause any damage to the components in the dryer (e.g. methanol, ethanol; note that DMF/DEF also can be used only if the dryer components are confirmed to be stable treated by DMF/DEF). The first step is similar to other conventional solvent-exchange processes, while here the organic solvents in the system are exchanged with liquid CO_2 below its critical temperature (31 ˚C) and above its critical pressure (73 bar). The difference is that this CO_2 exchange process is usually conducted between 0-10 ˚C, which is milder than conventional exchange processes conducted at room temperature. After several cycles of CO_2 exchange (typically a few hours for each cycle), the evaporation of CO_2 is carried out under its supercritical state. This is performed by depressurizing the liquid CO_2 above its critical temperature, which tremendously minimizes the surface tension during the process of liquid- to gas-phase transformation of CO_2 guests. As a result, the capillary stress exerted on the MOF structure is substantially decreased to preserve the delicate structure and its porosity. The sample is then quickly transferred to a sorption tube and run under dynamic vacuum with mild heat (< 50 ˚C) with the purpose of removing any potentially physisorbed CO_2 during the process.

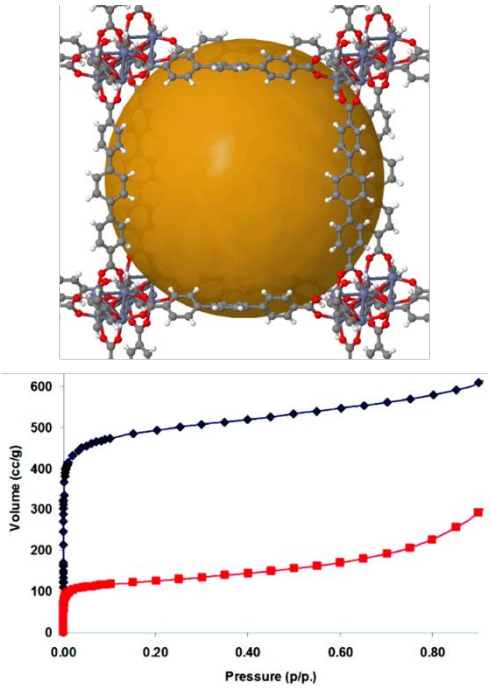

Figure 5. Top: Structure of IRMOF-16 (the bronze sphere indicates the void space in the structure). Bottom: N_2 isotherms of IRMOF-16 at 77 K after sc-CO_2 activation (black) and with $CHCl_3$ exchange by activation at 25 °C (red). Adapted with permission from ref. 45. Copyright 2009 American Chemical Society.

Since its first demonstration for MOF activation (Figure 5), sc-CO_2 has gained increasing attention, especially as a cost-effective and mild activation alternative for MOFs with low stability and/or high porosity, wherein the routinely used solvent-exchange with common organic solvents is found be

incapable of producing the theoretical surface areas based on their crystal structures.[45,111,112] In the past few years, numerous studies have proved the superiority of this method. For example, the MOFs mentioned above, SNU-70', UMCM-9, and FJI-1, were first activated by sc-CO_2 to obtain high BET areas of 5290, 4970, and 4813 $m^2 \cdot g^{-1}$, respectively.[113-115] Furthermore, full activation of NU-110, with one of the highest experimental BET surface areas of any porous materials, was accessed by the usage of sc-CO_2.[116] The Zhang group reported that they can obtain a high BET area of 5463 $m^2 \cdot g^{-1}$ for NPF-200 with tetrahedral linkers via sc-CO_2 activation. [117] Recently, our group applied this technique to activate a novel aluminum-based MOF, NU-1501-Al. As a result, the MOF presented a record-high BET area of 7310 $m^2\ g^{-1}$ while satisfying all four BET consistency criteria (9140 $m^2 g^{-1}$ if considering the first two) .[61] It is worth noting that a large number of MOFs with high BET area and large pore volume are activated through sc-CO_2 drying, demonstrating the generality of this promising activation protocol (Table 1 and Figure 3).[112] Matzger and coworkers also implemented the sc-CO_2 activation method into a flow system that directly activated a variety of MOFs from a DMF-solvated state and significantly reduced the time of the sc-CO_2 activation process.[118,119] For detailed procedures of sc-CO_2 activation of MOFs, the readers are directed to the literature.[45,61]

3.3 Other methods

While thermal activation is the most commonly used method, and sc-CO_2 activation has proven to be critical for the activation of high surface area MOFs, there are other activation methods that have been demonstrated in the literature as being effective for certain types of MOFs. Despite their limitations, these methods are worth considering with the compatible types of MOFs. Most of these efforts are devoted to facilitating the activation process while preserving the structural integrity of the MOFs. For example, among all the various methods of activating MOFs, a time-consuming solvent-exchange step is generally required, which can be potentially facilitated by a Soxhlet extraction and other suspension processing methods to benefit future industrial applications.[97,120]

3.3.1 **Freeze drying.** Freeze drying has been widely utilized in food processing, biological applications, and activation of porous materials.[121] In this process, the sample is first exchanged to a high-freezing-point solvent that is compatible with the MOF (e.g. benzene with a freezing point of 5.5 ˚C), and then cooled down to freeze the solvents. The frozen solvents can be subsequently removed under vacuum below its freezing point through sublimation, which effectively avoids surface tension that would otherwise be present during liquid-gas transformation. This method was first demonstrated in MOFs by Ma and co-workers in 2009 with benzene as the solvent, wherein a higher BET area of 1560 $m^2 \cdot g^{-1}$ (compared to 526 $m^2 \cdot g^{-1}$ *via* conventional vacuum-drying) of a representative mesoporous Cu-paddlewheel MOF was reported (Figure 6a).[122] While there are other successful examples of activating a pillared Fe-MOF and chitosan/UiO-66 by using benzene freeze drying,[123,124] some cases of structural collapse were also

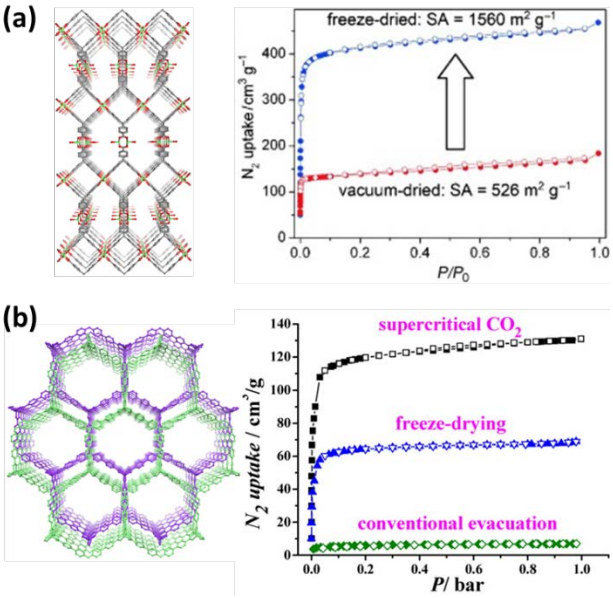

Figure 6. Crystal structure of Cu paddlewheel-based MOFs with its N_2 isotherms (a) and the 2-fold interpenetrated framework of FIR-3 with its N_2 isotherms obtained by different activation methods (b). Adapted with permission from ref. 122. Copyright 2009, Wiley-VCH Verlag GmbH & Co. KGaA, Weinheim. Adapted with permission from ref. 128. Copyright 2012, American Chemical Society.

observed; this was ascribed to the strong π–π interactions between the guest benzene molecules.[125-127] Due to the limited success and toxicity of benzene as the solvent, cyclohexane was later used for freeze drying of FIR-3 by Zhang and co-workers, wherein a much higher BET area (288 $m^2 \cdot g^{-1}$) than the one activated by conventional solvent-exchange was obtained (24 $m^2 \cdot g^{-1}$, Figure 6b).[128] In comparison, sc-CO_2 activation further preserved the porosity, resulting in the highest BET area of 544 $m^2 \cdot g^{-1}$ from all three activation methods.

3.3.2 **Microwave activation.** Microwave heating is a useful tool in a variety of chemical processes due to its ability to accelerate the reaction rate through the electromagnetic radiation. Compared to the conventional heat energy transfer by thermal diffusion, the microwave technique allows the energy to be directly transferred to the guest molecules in the fashion of wave penetration. In 2017, the Blight group first reported a microwave-assisted activation, wherein the MOFs (UiO-66, DUT-84, MOF-808) were pre-treated under microwave irradiation in water to remove the modulators that coordinated on the nodes.[129] However, limitations were found for this method as the treatment took place in water under high temperature; thus, this method is only applicable to MOFs which are water- and heat-stable. In addition, the authors reported the presence of remaining modulator on the nodes even after activation. In 2019, Jeong and coworkers reported a microwave activation (MA) where the coordinating and pore-filling solvents in the pristine MOFs (HKUST-1, UiO-66 and MOF-74) were efficiently removed.[130] The MOF crystallinity was retained while the BET area of HKUST-1 reaches 2000 $m^2 \cdot g^{-1}$ followed by only vacuum treatment (Figure 7). Furthermore, the time required for this activation process can be reduced to only 4 min if a solvent-exchange with methanol was performed

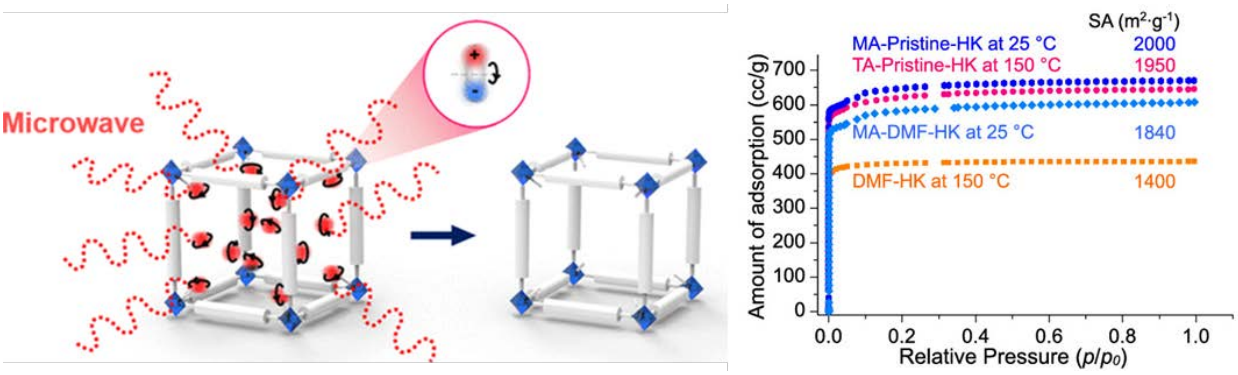

Figure 7. Left: schematic illustration of MOFs microwave activation; Right: N_2 adsorption isotherms comparison of thermally activated and microwave-activated DMF-HKUST-1 samples. Adapted with permission from ref. 130. Copyright 2019, American Chemical Society.

prior to the MA. Thus, this is a promising method for the efficient activation of MOFs that warrants further exploration.

3.3.3 **Chemical activation.** While guest solvents in the pores can be removed by the above-mentioned activation methods, some residual species such as modulators (i.e. benzoic acid, acetic acid) may remain coordinated to the metal nodes of the MOFs, preventing them from being eliminated through routine activation processes. Therefore, an additional chemical pre-treatment is required to unblock some pore space in order to obtain full access to the inner pore surface and, in some cases, release some open metal sites. Even though a few studies showed that high temperature (i.e. 200~250 ˚C) with dynamic vacuum can remove the residual bound modulators, these have been limited to low boiling point modulators such as formic acid, trifluoroacetic acid and acetic acid.[131,132] A more general pre-treatment with dilute hydrochloric acid —prior to the routine thermal activation—has proved successful for the activation of mesoporous Zr-based MOFs such as PCN-222 and NU-1000.[133,134] Mondloch *et. al.* revealed the role of HCl in cleaving the coordinated benzoic acid from the nodes through ^{1}H NMR and diffuse reflectance infrared Fourier transform spectroscopies (DRIFTS).[134] Later, this method was applied to the activation of MOFs such as NU-901,[135] NU-1200,[136] NU-1010[137] and PCN-608-OH[137]. This method is also transferable to removal of coordinated modulators in other Zr-carboxylate-based MOFs owing to their stability in dilute acidic conditions.

3.4 Common pitfalls in MOF activation

The complete activation of MOFs is of fundamental significance for understanding the correlation between MOF structure and various applications, which largely depends on being able to access the pores of the MOFs. While more stable MOFs are being discovered and protocols for proper activation of different types of MOFs are continually being established, caution should still be exercised, especially for novel MOFs, to avoid some common pitfalls in MOF activation. In general, incomplete activation and/or structural collapse will disguise the intrinsic properties of the MOFs and present them with an artificially lower BET area and pore volume than the expected values obtained from the crystal structures. While there are no universal protocols that will guarantee the complete activation of all MOFs, it is crucial to follow some empirical guidelines which can be customized to one's own needs.

3.4.1 **Incomplete exchange**. Since most MOFs can be effectively activated by the conventional solvent-exchange and thermal activation strategy, an adequate solvent exchange method is of great importance. Incomplete exchange will leave some unwanted high boiling point/surface tension solvents remaining in the pores, causing the structure to partially collapse during the thermal activation process or leaving the pores partially blocked if the conditions are not sufficient to remove the leftover solvents. Acetone and methanol are widely used in the literature to exchange high-boiling point solvents like DMF. The soaking/exchanging time as well as the frequency of exchange are important factor to ensure complete exchange, as demonstrated by Metzger and coworkers in their investigation of MOF-5 activation by exchanging DMF with CH_2Cl_2.[109] It was found that DMF can be rapidly exchanged by CH_2Cl_2 in the first 20 min while the exchanges after 20 min are not as significant. Regarding the frequency of exchange, it was shown that the BET area can increase to 3640 $m^2 \cdot g^{-1}$ (theoretical value of 3527 $cm^3 \cdot g^{-1}$) with three exchanges while only 2650 $m^2 \cdot g^{-1}$ was obtained after a single exchange (Figure 8, top). Wu and coworkers employed ^{1}H NMR for real-time monitoring of solvent exchange of DMF with benzene in MORF-1.[138] The results indicated a slow exchange rate as the ^{1}H NMR signal of DMF in the supernatant increased steadily in the first 10 h (Figure 8, bottom). Therefore, it is noted that exchange methods can differ significantly in different MOFs systems depending on their pore structure, stability and the compatibility of the two exchanging solvents.

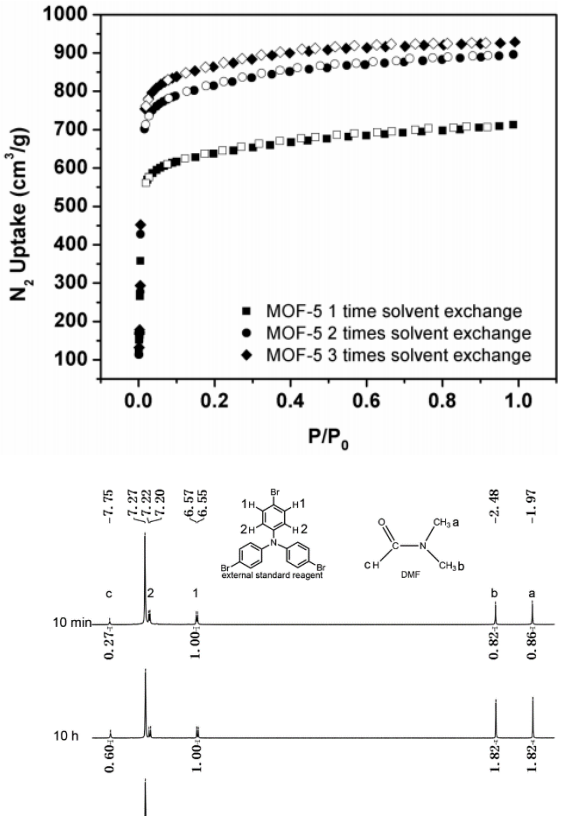

Figure 8. N_2 isotherms of MOF-5 with different solvent-exchange times (top) and ^1H NMR spectroscopy monitoring the amount of exchanged DMF in MORF-1 (Bottom). Reproduced with permission from ref. 109. Copyright 2017, Wiley-VCH Verlag GmbH & Co. KGaA, Weinheim. Reproduced with permission from ref. 138. Copyright 2018, Royal Society of Chemistry.

3.4.2 **Incomplete activation.** Following solvent-exchange, thermal activation under vacuum has been the most widely used method for MOF activation. Thermal activation is usually carried out at a temperature higher than the solvents' boiling points with dynamic vacuum for a certain time depending on the stability of the MOF and the properties of the residual solvents. Failure to completely remove residual solvents will result in lower BET area and pore volume than expected, especially in cases where there are coordinated solvent molecules on the metal nodes. For example, Dinca *et. al* reported that the residual DMF molecules in $Mo_3(BTC)_2$) (BTC stands for 1,3,5-benzentricarboxylate) can be more thoroughly removed by soaking the MOF in anhydrous methanol for prolonged time (i.e., 1 week). As a result, a more thorough activation of the MOF was achieved after thermal activation at 150 ˚C as evidenced by the higher BET area than previously reported (1689 vs 1280 m^2/g).[139] To ensure complete activation, analytical methods such as TGA, IR and NMR can be employed to assess the complete removal of residual guest molecules in the activated MOFs.

3.4.3 **Structural collapse**. A common consequence of improper activation is framework collapse. To guarantee that the structure integrity is retained and the samples are fully activated, the experimental results (surface area and pore volume) should be compared to the simulated results based on the single-crystal structures of other similar frameworks. A lower-than-expected BET area and/or decreased crystallinity after activation (as judged from PXRD) are indicative of incomplete activation or structural collapse. It is noted that PXRD should not be solely used as evidence for confirming the structural integrity of MOFs, as sometimes partial structural collapse may not be clearly visible through routine qualitative PXRD patterns. Therefore, a combination of analytical tools such as thermogravimetric analysis and mass spectrometry (TGA-MS), PXRD, SEM, NMR, and IR spectroscopy can be utilized to verify structural integrity and to detect residual solvent molecules, decomposition products, or other impurities after activation. Sometimes multiple trials will be needed to determine the optimal activation conditions before further studies.

4. General Strategies for Designing Porous MOFs

Based on the strength of metal-ligand bonds and the geometry of metal nodes and organic linkers, MOFs with different topologies and porosities can be achieved. Herein, a few general approaches for the design of MOFs with different pore systems are discussed with some representative examples highlighted.

A common analogy of designing MOFs is building tinker toys. Despite the oversimplification of this analogy, the underlying guidelines of reticular chemistry and the molecular building-block approach have made MOF chemistry accessible to an enormous number of researchers all over the world. By matching the geometries of the metal nodes and organic linkers, feasible topologies can be theoretically derived to aid the rational design of MOFs. A large established library of compatible geometries and MBBs can in turn assist with the computational discovery of MOFs.[140-142] This geometry matching strategy has been widely used in the design of MOFs owing to the well-defined structure and geometry of MOF building blocks via a reciprocal combination of experimental and computational studies.

4.1 Isoreticular expansion/contraction to control porosity

One commonly implemented method to control MOF porosity is the isoreticular expansion and/or contraction by altering their dimensions or chemical functionalities of the organic linker while maintaining the same underlying MOF topology.[7,52,59,143] Isoreticular control of MOF synthesis has multiple benefits, including the ability to realize higher porosity systems and to discover optimal pore sizes targeted for different applications such as gas storage[52,55] and catalysis.[144,145]

While a variety of isoreticular expansion/contraction studies have successfully achieved large pore volumes and apertures,[146] MOF-5 (also known as IRMOF-1) is a classic example where isoreticular control has been implemented to develop different pore sizes. MOF-5 is made up of octahedral Zn_4O clusters and 1,4-benzenedicarboxylate (BDC) linkers which self-assemble into a cubic network with CaB_6 topology.[147] By implementing alternative ditopic carboxylic-acid based linkers with different lengths and functionality, the isoreticular series of sixteen IRMOFs was established. In this way, the pore volume of each MOF in the series can thus be tuned to reach a maximum of about 90% free volume (Figure 9), keeping in mind the

functionalization or catenation in each MOF. MOF-5 has also been extended to MOF-1000, MOF-1001, MOF-1001A, and MOF-1002 by employing longer ditopic linkers with electron rich, 34- or 36-membered crown-ether receptor rings which act as molecular recognition sites for electron-poor substrates.[148] The isoreticular expansion of MOF-5 using these unique linkers with docking sites not only increased the percent unoccupied pore space from 79.2% (MOF-5/IRMOF-1) to 89% (MOF-1001), but also fostered charge transfer interactions between crown ether rings and paraquat molecules.

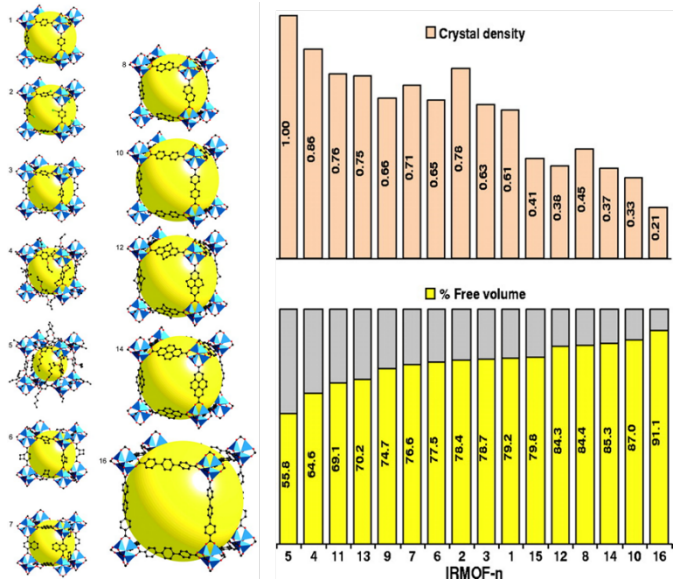

Figure 9. The crystal structures (left, the yellow spheres indicate the pore cavity), as well as the crystal densities and the percentage of free volumes (right) of the IRMOF series. Adapted with permission from ref. 147. Copyright 2002, American Association for the Advancement of Science.

One of the most prominent applications requiring highly porous MOFs is the adrosption and storage of gas molecules such as H_2, CH_4, CO_2, and O_2.[52,55] In this vein, isoreticular expansion has been widely used for achieving record-high BET area MOFs (Table 1) from known topologies. showed exceptionally high BET area and gas adsorption capacity. Recently, Farha reported the isoreticular expansion of NU-1500-Al by a single phenyl ring to NU-1501-Al with exceptionally high gravimetric and volumetric surface areas, optimal for clean energy H_2 and CH_4 storage.[61] NU-1500-Al is an *acs*-net MOF with 1.4 nm pores that is comprised of $[Al_3O]^{7-}$ nodes and a triptycene-based linker with *p*-phenylene carboxyl groups attached. By extending the ligand length by one phenyl ring, the BET area increases from 3560 m^2/g in NU-1500-Al to 7310 m^2/g in NU-1501-Al, the highest reported gravimetric uptake for all porous materials after satisfying all four BET consistency criteria. Remarkably, this isoreticular expansion results in a much higher absolute uptake and deliverable capacity of H_2 at 77K and 100 bar (NU-1500-Al: 8.2 wt%, NU-1501-Al: 14 wt%) while also maintaining nearly identical volumetric uptake (NU-1500-Al: 44.6 g/L, NU-1501-Al: 46.2 g/L). The isoreticular expansion of MOF-177 to MOF-200 also significantly increased the pore volume while decreasing the density of the MOFs, which is important for their use in gas storage tanks.[50] Thus, isoreticular control of MOFs is a very powerful technique, where even a small change can significantly tune MOF properties for a specific application.

Numerous other unique examples of porosity modulation by isoreticular control have also been established. For example, Rosi *et. al.* developed several MOFs based on bMOF-100 which exchange from shorter to longer ligands to generate a porosity gradient within a single MOF.[149] Since ligand exchange occurs from the outside to the inside of the crystal, the exchange can be stopped at different timepoints, resulting in MOFs with

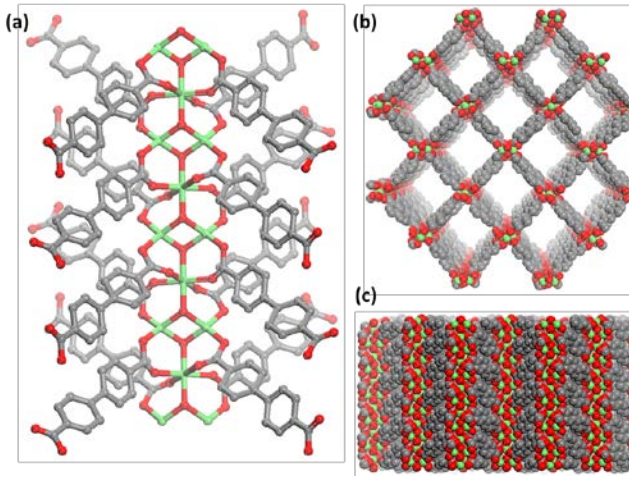

Figure 10. The structure of MOF-69A. (a). The rod-packing Zn-carboxylate SBU columns. (b). The open channels viewed along the *c* axis. (c) The "impenetrable wall" of linkers viewed along the *a* axis.

porosity gradients. Isoreticular control of porosity has also been extended to polymer-MOF hybrids (polyMOFs)[150] such as polyUiO-67 and polyUiO-68 derivatives, which increase in BET area from 618 m^2/g (polyUiO-67-8a-u) to 1626 m^2/g (polyUiO-68-10a-u) as well as even lanthanide-based MOFs.[151] Matzger and coworkers showed that the water stability of a series of MOFs isoreticular to MOF-5 was related to the pore sizes and linker hydrophobicity.[152] In addition, the NU-1000 to NU-1007 series of isoreticular MOFs based on Zr_6-cluster nodes and tetratopic carboxylate linkers showed tunable hierarchical pores that spans from 1.3 to 6.7 nm for the encapsulation of enzymes.[153]

4.2 Control of catenation

While isoreticular expansion of organic linkers often generates higher porosity MOFs, it can also result in catenated MOFs which will result in lower porosity.[147,148] Catenation is the entwining of multiple identical lattices such that the only method to separate the lattices is by breaking chemical bonds. While catenation in MOFs can be favorable for certain applications, it often prevent porosity gain since catenated lattices occupy the desired pore space. Thus, a variety of methods to control catenation and consequently retain MOF porosity have been developed such as mathematical construction, ligand design, reaction conditions, and novel synthetic methodologies.

Catenation can be mathematically forbidden through framework design,[146] such as the "infinite SBU" approach developed by Yaghi and coworkers.[154] The rod-packing framework, MOF-69A, is comprised of "infinite" Zn-O-C SBUs which are linked together by ditopic linkers. Because of this, the distance between linkers in the [001] direction is small, forming an "impenetrable wall" of pi-pi stacked phenyl rings (Figure 10), while the distance between carboxylate C atoms is much larger in the [110] direction. Through this design, long linkers can be used to create larger pores without the risk of catenation, since the "impenetrable" wall of linkers in the [001] directions metrically forbids catenation.[154]

Designing mathematically forbidden topologies has been the most successful strategy to avoid catenation and to achieve highly porous MOFs as exemplified by the *rht* topology.[52,155-158] recover the porosity.[161] Additionally, ligand length can be screened and tuned precisely to target the longest linker that results in a non-catenated framework.[162] Finally, linker conformation can also be modulated through torsion angle[163], or single/double bonds[164] to favor non-catenated MOFs. Kaskel and coworkers reported that by designing linkers with polar functional groups or using auxiliary cross-linkers, interpenetration in different MOFs was avoided to realize a highly porous MOF, DUT-60.[58,62,165]

Multiple reaction conditions in hydrothermal and solvothermal synthesis have been shown to control catenation such as modulator,[136,166,167] temperature,[168-170] reactant concentration,[147,171-173] and solvent.[174-178] For instance, NU-1200 (also known as BUT-12[179]) is a non-catenated, 8-connected, *the* topology MOF with the 4,4',4''-(2,4,6-

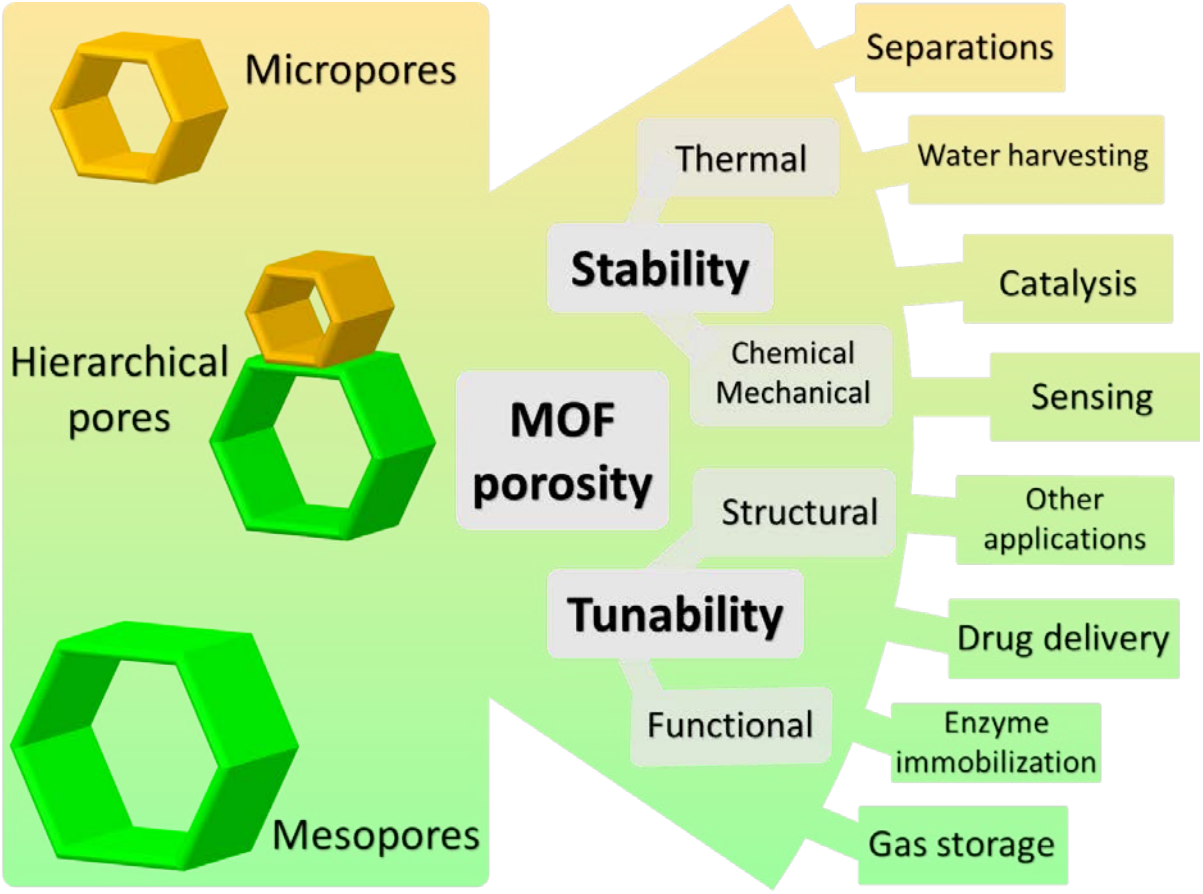

Scheme 2. Schematic overview of the porosity of MOFs, wherein their stability and tunability have enabled their utilization in various applications.

For instance, the NU-109, NU-100, NU-110 reticular series of MOFs exhibited exceptionally high BET areas and gas storage capacity, as interpenetration was precluded by the *rht* topology even when the arms of the hexatopic organic linker were expanded up to four phenyl rings and two acetyl groups in length.[56,60]

Ligand design and modification are also efficient methods to prevent catenation and preserve porosity. Ligands with bulkier substituents have been seen to impede catenation by occupying the pore space needed for catenated lattices,[159,160] and some of the bulky protecting groups on linkers which block catenation during synthesis MOF can be removed post-synthetically to trimethylbenzene-1,3,5-triyl)tribenzoic acid (TMTB) linker and Zr_6 node.[180] To synthesize NU-1200, benzoic acid is used as a modulator. However, when the less bulky modulator formic acid is implemented, a 2-fold catenated form of NU-1200, STA-26, is synthesized.[166] The mesoporous NU-1200 isotherm and pore volume of 1.42 cm^3/g can be compared to the microporous STA-26 isotherm and pore volume of 0.53 cm^3/g to deduce that bulkier modulators assist in preventing catenation and providing higher porosity. The effect of temperature and concentration was demonstrated in the SIFSIX-14-Cu-I system which exhibited partial 2-fold catenation of 70, 89, 93, and 99% at different temperatures and concentrations. These increasing

percentages of partial catenation also correspond to decreasing pore volumes of 252.7, 96.6, 68.9, and 23.5 cm^3/g at 77K.[172] It is surmised that non-catenation is favored by lower concentrations since it decreases the nucleation of catenated lattices within framework pores, and higher temperature often produce more thermodynamically stable, catenated frameworks.[171]

Finally, porosity can be retained through novel synthetic methodologies which prevent catenation, such as liquid phase epitaxial MOF growth. By implementing a 2D organic substrate that was alternatively immersed in a linker solution and a node solution, the commonly catenated MOF-508 (Zn node, BDC linker, and 4,4'-bipyridine pillars) with 4x4 Å channels was grown epitaxially as a non-catenated SURMOF (surface-mounted MOF) with 11x11 Å channels.[181] This functionalized substrate method allows for the growth of one lattice while suppressing the growth of the catenated lattice since it has no common nucleation plane with the substrate. Further developments in novel synthetic methodologies are desirable to expand the techniques available for catenation control and porosity preservation.

5. Strategies for Preserving MOF Porosity for Targeted Applications

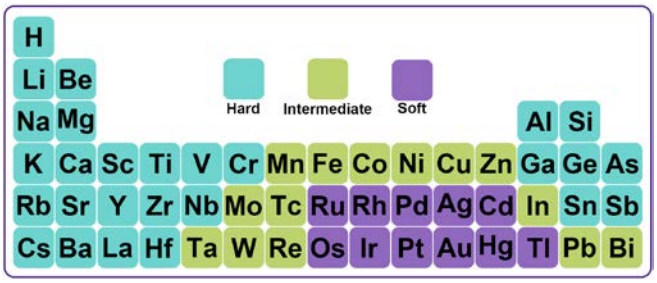

Figure 11. The classification of hard, soft, and intermediate acids within the periodic table.

Since porosity is the foundation for accessing MOF functionalities, preserving MOF porosity is vital for their performance in diverse applications.[41,182,183] To this end, stability is a major concern that has been accompanying the evolution of MOFs materials from a historical point of view.[8,184] Compared to traditional zeolites and porous carbon materials, MOFs exhibit much better performances towards many applications thanks to their high porosity, but may find limitations in applications that require high thermal, chemical, and water stabilities,[185-187] such as catalysis,[188,189] enzyme encapsulation,[190,191] and water capture.[79,192] Additionally, there are high demands of MOFs with tailorable porosity and functionality in order to optimize their performance for targeted applications (Scheme 2). While a few groups are at the forefront of synthesis and design of MOFs with novel structures and porosity, modification of known structures and topologies has been widely conducted for the utilization of MOFs in various applications. Herein, we will synopsize some representative strategies for preserving and altering the porosity of MOF materials with precise crystalline structures.

5.1 Stable metal-ligand bonds

One of the most important features that sets MOFs apart from earlier coordination polymers based on metal-neutral ligand bonds, is the presence of strong metal-charged ligand bonds; these result in enhanced stability and made permanent porosity possible in MOFs.[8] The metal nodes and deprotonated organic linkers can be considered as Lewis acid-base pairs and the strength of the coordination bonds between them can be estimated by the hard and soft acids and bases (HSAB) theory.[193,194] The coordination bonds between hard acid (metal ions with smaller ionic radius and higher oxidation state such as Zr^{4+} and Cr^{3+}, Figure 11) and hard base (the oxygen atoms in carboxylate linkers) will be much stronger than those between hard acid and softer base (neutral pyridine linkers). This results in Zr-MOFs and Cr-MOFs, such as Zr-UiO-66[91] and Cr-MIL-101[90], being among some of the most stable MOFs. Conversely, soft acid metal ions with larger ionic radius and lower oxidation states, such as Zn^{2+} and Ni^{2+}, they can form stable frameworks with charged soft base linkers like azolates, such as MFU-4,[195,196] MAF-X27,[197,198] PCN-601,[199] Co(BDP) (H_2BDP = 1,4-benzenedi(4'-pyrazolyl)),[200] and $M_3(BTP)_2$ (M = Ni, Cu, Zn and Co, H_3BTP = 1,3,5-tris(1*H*-pyrazol-4-yl)benzene)).[201] However, pairing hard acids and soft bases, or soft acids and hard bases usually give less stable MOFs, such as HKUST-1[202] and MOF-5.[46] Under the guidance of the HSAB theory, the stable pairs of metal ions and ligands can be easily to design MOF materials that meet the stability necessitated by the targeted application.

In addition to *de novo* synthesis, some kinetically labile metal-carboxylate coordination bonds can be strengthened by exchanging the metal ions to a harder metal ion, which will result in more kinetically inert metal-O bonds and thus stabilize the frameworks.[203-205] For example, Zhou and coworkers reported a post-synthetic metathesis and oxidation (PSMO) strategy to synthesize stable MOFs from MOFs with kinetically labile linkages such as Mg-carboxylate.[203] The original metal ions in the parent frameworks were first exchanged with precursors of hard metal ions bearing a lower oxidation state such as Fe(II) or Cr(II) in solution under inert atmosphere. The isostructural MOFs containing the new metal ions were then oxidized to form the kinetically more inert Fe(III)- or Cr(III)-O bonds (Figure 12). The PSMO process provides a facile and effective way to synthesize stable Cr-MOFs, which were otherwise challenging to be directly synthesized and crystallized

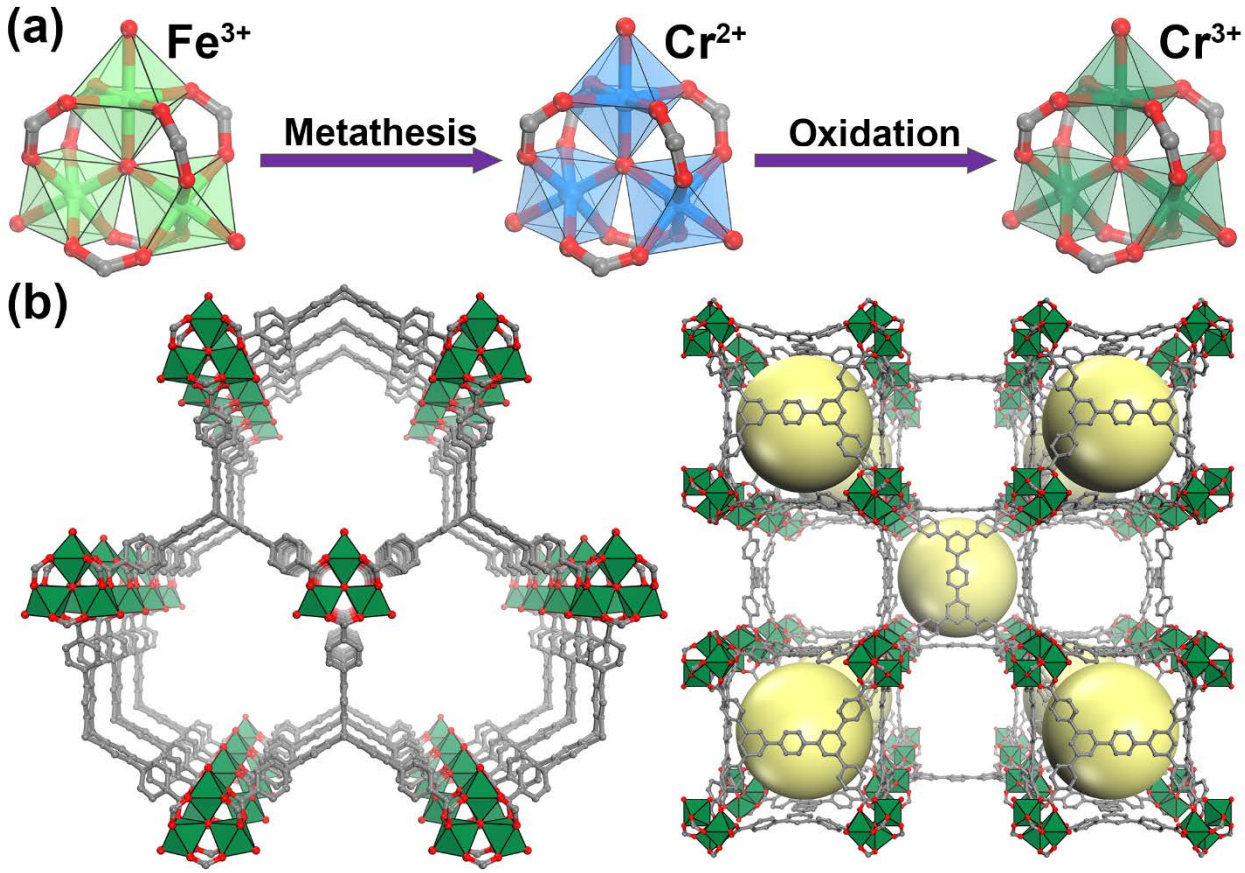

Figure 12. (a) Schematic diagram of metathesis-oxidation strategy of M_3-cluster. (b) Structures of NU-1500-Cr (left) and Cr-soc-MOF-1 (right). Color scheme: C (gray), O (red), Fe^{3+} (green), Cr^{2+} (blue), and Cr^{3+} (viridian).

due to kinetically inert Cr(III)-O bonds. The high water-stability of Cr-MOFs makes them promising candidates for water adsorption. Cr-soc-MOF-1[206] and NU-1500-Cr[207] were synthesized by PSMO of the Fe parent frameworks and showed excellent water capture capacity and stability after multiple adsorption/desorption cycles.

5.2 Linkers with enhanced stability

Besides the metal-linker bonds, the design and modification of linkers can also stabilize the final frameworks under certain conditions. For example, hydrophobic ligands inside the pores of MOFs can prevent water from coming into close proximity of metal-linker bonds, thus equipping the MOF with water stability. Commonly employed hydrophobic functional groups, such as fluoride, alkyl, and aromatic groups, can be incorporated in MOFs through isoreticular substitution, *de novo* design or post-synthetic modification (Figure 13). Isoreticular substitution of some parent MOFs built from otherwise unstable metal-linker bonds with hydrophobic linkers can improve their water stability compared to the parent structures built from otherwise unstable metal-linker bonds in the presence of water (Figure 14). For instance, MOF-5 ($[Zn_4O(COO^-)_6]$) is unstable under the attack of water, and its pore structures will collapse under humid conditions. However, after grafting of hydrophobic moieties such as trifluoromethoxy and methyl groups on the BDC linker, the porosity of modified MOF-5 can be preserved after days of exposure to ambient air.[208,209] Another class of MOFs that suffers from water instability is based on metal $[M_2(COO^-)_4]$ (M = Co^{2+}, Ni^{2+}, Cu^{2+}, and Zn^{2+}) paddlewheel SBUs. The introduction of hydrophobic groups provided a shield to protect the paddlewheel from hydrolysis and enhance the water stability.[210-212] Through multiple cycles of water adsorption tests, the condensation points of methylated and fluorinated MOFs are at higher relative humidity, confirming that the frameworks are more hydrophobic than their parent structures.

Even if the metal-ligand bond is already stable in water, a hydrophobic linker can further alter the hydrophobicity of frameworks for targeted applications. For the capture of volatile organic compounds (VOCs) in air, moisture is unavoidable and will act as a competitor during the adsorption process. Thus, avoiding water adsorption is important for such applications. Cr-MIL-101 is known as a stable framework even under harsh conditions, but it can adsorb about 70 mmol/g of water within the relative humidity range of 40-60% at room temperature, hindering the further capture of VOCs under such conditions. To avoid water adsorption, 1,4-naphthalene dicarboxylic acid, instead of H_2BDC, was used to construct *mtn* network MIL(Cr)-Z1, which adsorbed only about 17 mmol/g of water up to 90% relative humidity at RT.[213] As a result, MIL(Cr)-Z1 avoided the interference of water during the capture of VOCs, and enhanced the adsorption capacity and selectivity simultaneously. The same strategy was used in the *fcu* frameworks constructed by $[Ni_8(OH)_4(H_2O)_2Pz_{12}]$ nodes. The linear pyrazolate-based ligand was modified by introducing methyl and trifluoromethyl group.[214] This resulted in a significant increase in hydrophobicity, thus overcoming the

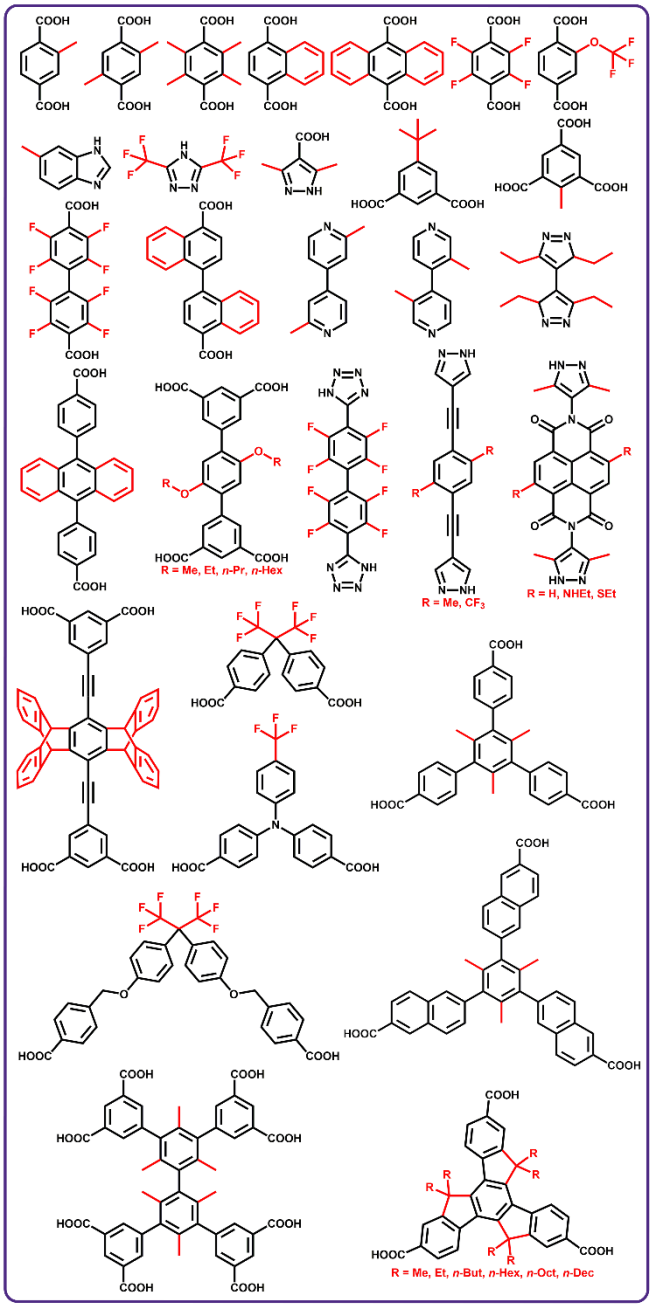

Figure 13. The chemical structure of hydrophobic organic linkers in which the hydrophobic groups are marked with red color.

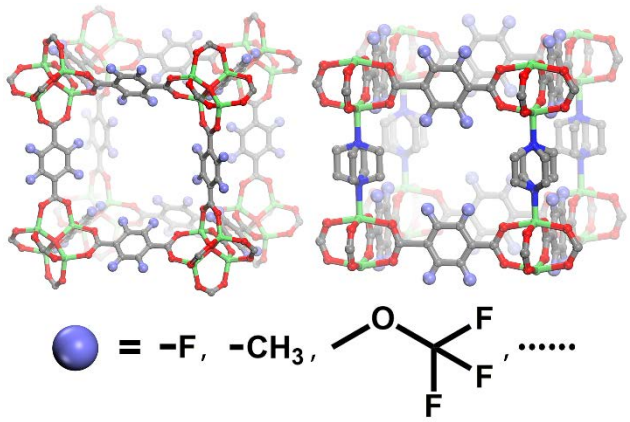

Figure 14. Schematic view of the construction of hydrophobic MOFs by introducing hydrophobic groups onto organic linkers *via* reticular chemistry. Color scheme: metal (green), C (gray), O (red), N (blue), and hydrophobic groups (purple).

issues associated with the capture of VOCs in highly competitive, moist environments.

The application of MOFs in catalysis usually involves acidic or alkaline environment, in which case the acid and base chemical stability is also crucial for MOFs. In the case of JUC-1000, an organic ligand containing both acidic and basic functional groups was designed and used to construct Cu paddle-wheel based MOFs .[215] The ligand can act as a buffer where the phenol group is a weak acid, with the amino and triazine groups serving as weak bases; these then withstand both the attack of acid and base. JUC-1000 can maintain its porosity in both acidic (pH = 1.5) and basic (pH = 12.5) aqueous solutions. With the benefit of the acid–base-paired ligand, JUC-1000 exhibited excellent performance in the chemical fixation of carbon dioxide at ambient conditions.

Post-synthetic modification (PSM) of MOF linkers is an effective method to preserve the porosity of MOFs by either strengthening unstable bonds or modifying hydrophobicity. PSM can also be employed to fortify unstable organic linkers. For example, the imine bonds in the linker of NU-401 are prone to hydrolysis under moist conditions. To stabilize the linker, an aza-Diels-Alder reaction was used to transform the unstable C=N bond into a rigid and stable quinoline group.[216] The post-synthetically modified framework NU-401-Q (Q = quinoline) exhibited enhanced water stability after and improved oxygen adsorption capacity compared to the parent NU-401.

6. Conclusions and Outlooks

The past few decades have witnessed the rapid growth of MOF research both in the development of new materials and the utilization of these highly programmable materials for a wide range of applications. Since porosity is a fundamental characteristic of MOFs and a foundation for the majority of MOF applications, research into the design and control of porosity, including how to best preserve porosity for a targeted application, has been a central theme. Looking forward, this theme will be continued in order to better control the accessibility of the void space and the functionalities within the frameworks.

One of the ongoing challenges is the design and synthesis of highly porous MOFs that can balance both gravimetric and volumetric surface areas; these types of adsorbents are in high demand for on-board storage and delivery of clean fuels, such as hydrogen and methane gases.

Additionally, the ability to make high porosity MOFs that require minimal processing has always been appealing for their practical applications. Simplifying the time- and energy-consuming process of MOF activation towards a direct activation through heat and vacuum without a solvent-exchange pretreatment remains a challenge. Even more appealing is the possibility of synthesizing these highly porous MOFs with simple and cost-effective organic linkers. Generally, the quest for more stable materials is always of high interest over the long term due to their durability, reusability, and cost efficiency.

The great promise of using MOFs as host materials is not limited to small gas molecules. MOFs have already shown promise for encapsulation of large molecules such as pharmaceuticals, proteins, polyoxometalates and molecular magnets, and there still remains vast unchartered land to be explored with the compass of reticular chemistry. From a historical point of view, the field of MOF research has been prospering and the road ahead will be rife with challenges. Nevertheless, along with the challenges is a bright future with plenty of opportunity.

Conflicts of interest

There are no conflicts to declare.

Acknowledgements

O.K.F. acknowledges support from the U. S. Department of Energy's Office of Energy Efficiency and Renewable Energy (EERE) under award no. DE-EE0008816; the U. S. Department of Energy (DOE) Office of Science, Basic Energy Sciences Program for Separation (DE-FG02-08ER15967); the Northwestern University Institute for Catalysis in Energy Processes (ICEP), funded by the DOE, Office of Basic Energy Sciences (Award Number DE-FG02-03ER15457), and Northwestern University; the U.S. Department of Energy, National Nuclear Security Administration, under Award Number DE-NA0003763. O.K.F. gratefully acknowledges Northwestern University for the financial support. S.L.H. acknowledges support from the U.S. Department of Energy, National Nuclear Security Administration Stewardship Science Graduate Fellowship.

Notes and references

1. M. E. Davis, *Nature*, 2002, **417**, 813-821.
2. M. E. Davis, C. Saldarriaga, C. Montes, J. Garces and C. Crowdert, *Nature*, 1988, **331**, 698-699.
3. C. T. Kresge, M. E. Leonowicz, W. J. Roth, J. C. Vartuli and J. S. Beck, *Nature*, 1992, **359**, 710-712.

4. O. M. Yaghi and H. Li, *J. Am. Chem. Soc.*, 1995, **117**, 10401-10402.
5. O. M. Yaghi, G. Li and H. Li, *Nature*, 1995, **378**, 703-706.
6. H. Li, M. Eddaoudi, T. L. Groy and O. M. Yaghi, *J. Am. Chem. Soc.*, 1998, **120**, 8571-8572.
7. M. Eddaoudi, J. Kim, N. Rosi, D. Vodak, J. Wachter, M. O'Keeffe and O. M. Yaghi, *Science*, 2002, **295**, 469-472.
8. C. Gropp, S. Canossa, S. Wuttke, F. Gándara, Q. Li, L. Gagliardi and O. M. Yaghi, *ACS Cent. Sci.*, 2020, 10.1021/acscentsci.0c00592.
9. A. Li, R. Bueno-Perez, S. Wiggin and D. Fairen-Jimenez, *CrystEngComm*, 2020, 10.1039/D0CE00299B.
10. P. Z. Moghadam, A. Li, S. B. Wiggin, A. Tao, A. G. P. Maloney, P. A. Wood, S. C. Ward and D. Fairen-Jimenez, *Chem. Mater.*, 2017, **29**, 2618-2625.
11. *While this "MOF subset" includes "1D, 2D, and 3D MOF and MOF-like structures with all kinds of pore sizes as well as nonporous structures" according to reference 10, IUPAC defines MOF as "a Coordination Polymer (or alternatively Coordination Network) with an open framework containing potential voids" (See Pure Appl. Chem., 2013, 85, 1715).Therefore, the number of structures in the "MOF subset" would be larger than those recommended by IUPAC.*
12. N. L. Rosi, J. Eckert, M. Eddaoudi, D. T. Vodak, J. Kim, M. O'Keeffe and O. M. Yaghi, *Science*, 2003, **300**, 1127-1129.
13. J.-R. Li, J. Sculley and H.-C. Zhou, *Chem. Rev.*, 2012, **112**, 869-932.
14. B. Chen, C. Liang, J. Yang, D. S. Contreras, Y. L. Clancy, E. B. Lobkovsky, O. M. Yaghi and S. Dai, *Angew. Chem., Int. Ed.*, 2006, **45**, 1390-1393.
15. X. Cui, K. Chen, H. Xing, Q. Yang, R. Krishna, Z. Bao, H. Wu, W. Zhou, X. Dong, Y. Han, B. Li, Q. Ren, M. J. Zaworotko and B. Chen, *Science*, 2016, **353**, 141-144.
16. J. Lee, O. K. Farha, J. Roberts, K. A. Scheidt, S. T. Nguyen and J. T. Hupp, *Chem. Soc. Rev.*, 2009, **38**, 1450-1459.
17. X. Zhang, Z. Huang, M. Ferrandon, D. Yang, L. Robison, P. Li, T. C. Wang, M. Delferro and O. K. Farha, *Nat. Catal.*, 2018, **1**, 356-362.
18. T. Zhang and W. Lin, *Chem. Soc. Rev.*, 2014, **43**, 5982-5993.
19. L. Jiao and H.-L. Jiang, *Chem*, 2019, **5**, 786-804.
20. B. Chen, Y. Yang, F. Zapata, G. Lin, G. Qian and E. B. Lobkovsky, *Adv. Mater.*, 2007, **19**, 1693-1696.
21. L. E. Kreno, K. Leong, O. K. Farha, M. Allendorf, R. P. Van Duyne and J. T. Hupp, *Chem. Rev.*, 2012, **112**, 1105-1125.
22. Y. Chen, P. Li, H. Noh, C. W. Kung, C. T. Buru, X. Wang, X. Zhang and O. K. Farha, *Angew. Chem., Int. Ed.*, 2019, **58**, 7682-7686.
23. X. Lian, Y. Fang, E. Joseph, Q. Wang, J. Li, S. Banerjee, C. Lollar, X. Wang and H.-C. Zhou, *Chem. Soc. Rev.*, 2017, **46**, 3386-3401.
24. Y. Chen, P. Li, J. Zhou, C. T. Buru, L. Dordevic, P. Li, X. Zhang, M. M. Cetin, J. F. Stoddart, S. I. Stupp, M. R. Wasielewski and O. K. Farha, *J. Am. Chem. Soc.*, 2020, **142**, 1768-1773.
25. M.-X. Wu and Y.-W. Yang, *Adv. Mater.*, 2017, **29**, 1606134.
26. Y. Chen, P. Li, J. A. Modica, R. J. Drout and O. K. Farha, *J. Am. Chem. Soc.*, 2018, **140**, 5678-5681.
27. L. Sun, M. G. Campbell and M. Dincă, *Angew. Chem., Int. Ed.*, 2016, **55**, 3566-3579.
28. W. Xu, X. Pei, C. S. Diercks, H. Lyu, Z. Ji and O. M. Yaghi, *J. Am. Chem. Soc.*, 2019, **141**, 17522-17526.
29. X. Zhang, M. R. Saber, A. P. Prosvirin, J. H. Reibenspies, L. Sun, M. Ballesteros-Rivas, H. Zhao and K. R. Dunbar, *Inorg. Chem. Front.*, 2015, **2**, 904-911.
30. G. Mínguez Espallargas and E. Coronado, *Chem. Soc. Rev.*, 2018, **47**, 533-557.
31. D. Aulakh, H. Xie, Z. Shen, A. Harley, X. Zhang, A. A. Yakovenko, K. R. Dunbar and M. Wriedt, *Inorg Chem*, 2017, **56**, 6965-6972.
32. B. F. Hoskins and R. Robson, *J. Am. Chem. Soc.*, 1989, **111**, 5962-5964.
33. B. F. Hoskins and R. Robson, *J. Am. Chem. Soc.*, 1990, **112**, 1546-1554.
34. M. Kondo, T. Yoshitomi, H. Matsuzaka, S. Kitagawa and K. Seki, *Angew. Chem., Int. Ed.*, 1997, **36**, 1725-1727.
35. O. M. Yaghi, M. O'Keeffe, N. W. Ockwig, H. K. Chae, M. Eddaoudi and J. Kim, *Nature*, 2003, **423**, 705-714.
36. N. W. Ockwig, O. Delgado-Friedrichs, M. O'Keeffe and O. M. Yaghi, *Acc. Chem. Res.*, 2005, **38**, 176-182.
37. O. M. Yaghi, *ACS Cent. Sci.*, 2019, **5**, 1295-1300.
38. O. M. Yaghi, M. J. Kalmutzki and C. S. Diercks, in *Introduction to Reticular Chemistry*, John Wiley and Sons 2019, 10.1002/9783527821099.ch1.
39. Z. Chen, H. Jiang, M. Li, M. O'Keeffe and M. Eddaoudi, *Chem. Rev.*, 2020, 10.1021/acs.chemrev.9b00648.
40. M. O'Keeffe, M. A. Peskov, S. J. Ramsden and O. M. Yaghi, *Acc. Chem. Res.*, 2008, **41**, 1782-1789.
41. O. K. Farha and J. T. Hupp, *Acc. Chem. Res.*, 2010, **43**, 1166-1175.
42. A. J. Howarth, A. W. Peters, N. A. Vermeulen, T. C. Wang, J. T. Hupp and O. K. Farha, *Chem. Mater.*, 2017, **29**, 26-39.
43. S. S. Kaye, A. Dailly, O. M. Yaghi and J. R. Long, *J. Am. Chem. Soc.*, 2007, **129**, 14176-14177.
44. P. L. Llewellyn, S. Bourrelly, C. Serre, A. Vimont, M. Daturi, L. Hamon, G. De Weireld, J.-S. Chang, D.-Y. Hong, Y. Kyu Hwang, S. Hwa Jhung and G. Férey, *Langmuir*, 2008, **24**, 7245-7250.
45. A. P. Nelson, O. K. Farha, K. L. Mulfort and J. T. Hupp, *J. Am. Chem. Soc.*, 2009, **131**, 458-460.
46. H. Li, M. Eddaoudi, M. O'Keeffe and O. M. Yaghi, *Nature*, 1999, **402**, 276-279.
47. G. Férey, C. Mellot-Draznieks, C. Serre, F. Millange, J. Dutour, S. Surblé and I. Margiolaki, *Science*, 2005, **309**, 2040-2042.
48. J. An, O. K. Farha, J. T. Hupp, E. Pohl, J. I. Yeh and N. L. Rosi, *Nat. Commun.*, 2012, **3**, 604.
49. N. Klein, I. Senkovska, K. Gedrich, U. Stoeck, A. Henschel, U. Mueller and S. Kaskel, *Angew. Chem., Int. Ed.*, 2009, **48**, 9954-9957.
50. H. Furukawa, N. Ko, Y. B. Go, N. Aratani, S. B. Choi, E. Choi, A. Ö. Yazaydin, R. Q. Snurr, M. O'Keeffe, J. Kim and O. M. Yaghi, *Science*, 2010, **329**, 424-428.
51. H. Furukawa, M. A. Miller and O. M. Yaghi, *J. Mater. Chem.*, 2007, **17**, 3197-3204.
52. D. Yuan, D. Zhao, D. Sun and H.-C. Zhou, *Angew. Chem., Int. Ed.*, 2010, **49**, 5357-5361.
53. K. Koh, A. G. Wong-Foy and A. J. Matzger, *J. Am. Chem. Soc.*, 2009, **131**, 4184-4185.
54. U. Stoeck, S. Krause, V. Bon, I. Senkovska and S. Kaskel, *Chem. Commun.*, 2012, **48**, 10841-10843.
55. D. Alezi, Y. Belmabkhout, M. Suyetin, P. M. Bhatt, Ł. J. Weseliński, V. Solovyeva, K. Adil, I. Spanopoulos, P. N. Trikalitis, A.-H. Emwas and M. Eddaoudi, *J. Am. Chem. Soc.*, 2015, **137**, 13308-13318.
56. O. K. Farha, A. Özgür Yazaydın, I. Eryazici, C. D. Malliakas, B. G. Hauser, M. G. Kanatzidis, S. T. Nguyen, R. Q. Snurr and J. T. Hupp, *Nat. Chem.*, 2010, **2**, 944-948.

57. U. Stoeck, I. Senkovska, V. Bon, S. Krause and S. Kaskel, *Chem. Commun.*, 2015, **51**, 1046-1049.
58. R. Grünker, V. Bon, P. Müller, U. Stoeck, S. Krause, U. Mueller, I. Senkovska and S. Kaskel, *Chem. Commun.*, 2014, **50**, 3450-3452.
59. T. C. Wang, W. Bury, D. A. Gómez-Gualdrón, N. A. Vermeulen, J. E. Mondloch, P. Deria, K. Zhang, P. Z. Moghadam, A. A. Sarjeant, R. Q. Snurr, J. F. Stoddart, J. T. Hupp and O. K. Farha, *J. Am. Chem. Soc.*, 2015, **137**, 3585-3591.
60. O. K. Farha, I. Eryazici, N. C. Jeong, B. G. Hauser, C. E. Wilmer, A. A. Sarjeant, R. Q. Snurr, S. T. Nguyen, A. Ö. Yazaydın and J. T. Hupp, *Journal of the American Chemical Society*, 2012, **134**, 15016-15021.
61. Z. Chen, P. Li, R. Anderson, X. Wang, X. Zhang, L. Robison, L. R. Redfern, S. Moribe, T. Islamoglu, D. A. Gómez-Gualdrón, T. Yildirim, J. F. Stoddart and O. K. Farha, *Science*, 2020, **368**, 297-303.
62. I. M. Hönicke, I. Senkovska, V. Bon, I. A. Baburin, N. Bönisch, S. Raschke, J. D. Evans and S. Kaskel, *Angew. Chem., Int. Ed.*, 2018, **57**, 13780-13783.
63. A. P. Shevchenko, E. V. Alexandrov, A. A. Golov, O. A. Blatova, A. S. Duyunova and V. A. Blatov, *Chem. Commun.*, 2020, **56**, 9616-9619.
64. J. Rouquerol, D. Avnir, C. W. Fairbridge, D. H. Everett, J. M. Haynes, N. Pernicone, J. D. F. Ramsay, K. S. W. Sing and K. K. Unger, *Pure Appl. Chem.*, 1994, **66**, 1739.
65. K. S. Sing, D. H. Everett, R. Haul, L. Moscou, R. A. Pierotti, J. Rouquerol and T. Siemieniewska, *Pure Appl. Chem*, 1985, **57**, 603-619.
66. T. Matthias, K. Katsumi, V. N. Alexander, P. O. James, R.-R. Francisco, R. Jean and S. W. S. Kenneth, *Pure Appl. Chem.*, 2015, **87**, 1051-1069.
67. M. Thommes, K. Kaneko, A. V. Neimark, J. P. Olivier, F. Rodriguez-Reinoso, J. Rouquerol and K. S. W. Sing, *Pure Appl. Chem.*, 2015, **87**, 1051.
68. R. Kitaura, K. Seki, G. Akiyama and S. Kitagawa, *Angew. Chem. Int. Ed.*, 2003, **42**, 428-430.
69. J. H. Lee, S. Jeoung, Y. G. Chung and H. R. Moon, *Coord. Chem. Rev.*, 2019, **389**, 161-188.
70. J.-P. Zhang, H.-L. Zhou, D.-D. Zhou, P.-Q. Liao and X.-M. Chen, *Natl. Sci. Rev.*, 2017, **5**, 907-919.
71. A. Schneemann, V. Bon, I. Schwedler, I. Senkovska, S. Kaskel and R. A. Fischer, *Chem. Soc. Rev.*, 2014, **43**, 6062-6096.
72. Z.-J. Lin, J. Lu, M. Hong and R. Cao, *Chem. Soc. Rev.*, 2014, **43**, 5867-5895.
73. K. Uemura, R. Matsuda and S. Kitagawa, *J. Solid State Chem.*, 2005, **178**, 2420-2429.
74. J. A. Mason, J. Oktawiec, M. K. Taylor, M. R. Hudson, J. Rodriguez, J. E. Bachman, M. I. Gonzalez, A. Cervellino, A. Guagliardi, C. M. Brown, P. L. Llewellyn, N. Masciocchi and J. R. Long, *Nature*, 2015, **527**, 357-361.
75. K. A. Cychosz and M. Thommes, *Engineering*, 2018, **4**, 559-566.
76. N. Hanikel, M. S. Prévot and O. M. Yaghi, *Nature Nanotechnology*, 2020, **15**, 348-355.
77. F.-X. Coudert, *Acc. Chem. Res.*, 2020, **53**, 1342-1350.
78. H. Furukawa, F. Gándara, Y.-B. Zhang, J. Jiang, W. L. Queen, M. R. Hudson and O. M. Yaghi, *J. Am. Chem. Soc.*, 2014, **136**, 4369-4381.
79. J. Canivet, A. Fateeva, Y. Guo, B. Coasne and D. Farrusseng, *Chem. Soc. Rev.*, 2014, **43**, 5594-5617.
80. S. Brunauer, P. H. Emmett and E. Teller, *J. Am. Chem. Soc.*, 1938, **60**, 309-319.
81. P. Llewellyn, G. Maurin and J. Rouquerol, in *Adsorption by Powders and Porous Solids (Second Edition)*, Academic Press, Oxford, 2014, https://doi.org/10.1016/B978-0-08-097035-6.00014-0, pp. 565-610.
82. J. L. Rouquerol, P.; Rouquerol, F., ed. P. L. R.-R. Llewellyn, F.; Rouquerol, J.; Seaton, N., Eds, Elsevier, Amsterdam, 2007, vol. 160, p. 49.
83. D. A. Gómez-Gualdrón, P. Z. Moghadam, J. T. Hupp, O. K. Farha and R. Q. Snurr, *J. Am. Chem. Soc.*, 2016, **138**, 215-224.
84. Z. Chen, P. Li, X. Wang, K.-i. Otake, X. Zhang, L. Robison, A. Atilgan, T. Islamoglu, M. G. Hall, G. W. Peterson, J. F. Stoddart and O. K. Farha, *J. Am. Chem. Soc.*, 2019, **141**, 12229-12235.
85. J. Rouquerol, F. Rouquerol, P. Llewellyn, G. Maurin and K. S. Sing, *Adsorption by powders and porous solids: principles, methodology and applications*, Academic press, 2014.
86. S. Lowell, J. E. Shields, M. A. Thomas and M. Thommes, *Characterization of porous solids and powders: surface area, pore size and density*, Springer Science & Business Media, 2012.
87. T. F. Willems, C. H. Rycroft, M. Kazi, J. C. Meza and M. Haranczyk, *Microporous Mesoporous Mater.*, 2012, **149**, 134-141.
88. J. S. S. Lowell, M. A. Tomas and M. Thommes, *Characterization of Porous Solids and Powders: Surface Area, Pore Size and Density*, Springer, 2004.
89. M. Thommes and K. A. Cychosz, *Adsorption*, 2014, **20**, 233-250.
90. G. Férey, C. Mellot-Draznieks, C. Serre, F. Millange, J. Dutour, S. Surblé and I. Margiolaki, *Science*, 2005, **309**, 2040.
91. J. H. Cavka, S. Jakobsen, U. Olsbye, N. Guillou, C. Lamberti, S. Bordiga and K. P. Lillerud, *J. Am. Chem. Soc.*, 2008, **130**, 13850-13851.
92. B. Mu, C.-X. Li, M. Song, Y.-L. Ren and R.-D. Huang, *CrystEngComm*, 2016, **18**, 3086-3094.
93. J. E. Efome, D. Rana, T. Matsuura and C. Q. Lan, *ACS Appl Mater Interfaces*, 2018, **10**, 18619-18629.
94. Y.-P. He, L.-B. Yuan, H. Xu and J. Zhang, *Cryst. Growth Des.*, 2016, **17**, 290-294.
95. D. Alezi, Y. Belmabkhout, M. Suyetin, P. M. Bhatt, L. J. Weselinski, V. Solovyeva, K. Adil, I. Spanopoulos, P. N. Trikalitis, A. H. Emwas and M. Eddaoudi, *J. Am. Chem. Soc.*, 2015, **137**, 13308-13318.
96. D. J. Tranchemontagne, J. R. Hunt and O. M. Yaghi, *Tetrahedron*, 2008, **64**, 8553-8557.
97. G. Wißmann, A. Schaate, S. Lilienthal, I. Bremer, A. M. Schneider and P. Behrens, *Microporous Mesoporous Mater.*, 2012, **152**, 64-70.
98. S. Yuan, W. Lu, Y. P. Chen, Q. Zhang, T. F. Liu, D. Feng, X. Wang, J. Qin and H. C. Zhou, *J. Am. Chem. Soc.*, 2015, **137**, 3177-3180.
99. V. Bon, V. Senkovskyy, I. Senkovska and S. Kaskel, *Chem. Commun.*, 2012, **48**, 8407-8409.
100. L.-H. Xie, X.-M. Liu, T. He and J.-R. Li, *Chem*, 2018, **4**, 1911-1927.
101. D. Feng, K. Wang, J. Su, T. F. Liu, J. Park, Z. Wei, M. Bosch, A. Yakovenko, X. Zou and H. C. Zhou, *Angew. Chem., Int. Ed.*, 2015, **54**, 149-154.
102. Y. Wang, M. He, X. Gao, S. Li and Y. He, *Dalton Trans.*, 2018, **47**, 7213-7221.
103. M.-Y. Chao, J. Chen, X.-Y. Wu, R.-Y. Wang, P.-P. Wang, L. Ding, D. J. Young and W.-H. Zhang, *ChemPlusChem*, 2020, **85**, 503-509.
104. H. Yang, T. X. Trieu, X. Zhao, Y. Wang, Y. Wang, P. Feng and X. Bu, *Angew. Chem., Int. Ed.*, 2019, **58**, 11757-11762.

105. S. Yuan, L. Huang, Z. Huang, D. Sun, J. S. Qin, L. Feng, J. Li, X. Zou, T. Cagin and H. C. Zhou, *J. Am. Chem. Soc.*, 2020, **142**, 4732-4738.
106. L. Feng, S. Yuan, J.-S. Qin, Y. Wang, A. Kirchon, D. Qiu, L. Cheng, S. T. Madrahimov and H.-C. Zhou, *Matter*, 2019, **1**, 156-167.
107. J. S. Choi, J. Bae, E. J. Lee and N. C. Jeong, *Inorg Chem*, 2018, **57**, 5225-5231.
108. T. Y. Luo, P. Das, D. L. White, C. Liu, A. Star and N. L. Rosi, *J. Am. Chem. Soc.*, 2020, **142**, 2897-2904.
109. J. Ma, A. P. Kalenak, A. G. Wong-Foy and A. J. Matzger, *Angew. Chem., Int. Ed.*, 2017, **56**, 14618-14621.
110. A. I. Cooper, *Adv. Mater.*, 2003, **15**, 1049-1059.
111. A. J. Howarth, A. W. Peters, N. A. Vermeulen, T. C. Wang, J. T. Hupp and O. K. Farha, *Chem. Mater.*, 2016, **29**, 26-39.
112. J. E. Mondloch, O. Karagiaridi, O. K. Farha and J. T. Hupp, *CrystEngComm*, 2013, **15**.
113. T. K. Prasad and M. P. Suh, *Chemistry*, 2012, **18**, 8673-8680.
114. K. Koh, J. D. Van Oosterhout, S. Roy, A. G. Wong-Foy and A. J. Matzger, *Chem. Sci.*, 2012, **3**.
115. B. Liu, A. G. Wong-Foy and A. J. Matzger, *Chem. Commun.*, 2013, **49**, 1419-1421.
116. O. K. Farha, I. Eryazici, N. C. Jeong, B. G. Hauser, C. E. Wilmer, A. A. Sarjeant, R. Q. Snurr, S. T. Nguyen, A. O. Yazaydin and J. T. Hupp, *J. Am. Chem. Soc.*, 2012, **134**, 15016-15021.
117. X. Zhang, X. Zhang, J. A. Johnson, Y. S. Chen and J. Zhang, *J. Am. Chem. Soc.*, 2016, **138**, 8380-8383.
118. K. Koh, J. D. Van Oosterhout, S. Roy, A. G. Wong-Foy and A. J. Matzger, *Chem. Sci.*, 2012, **3**, 2429-2432.
119. B. Liu, A. G. Wong-Foy and A. J. Matzger, *Chem. Commun.*, 2013, **49**, 1419-1421.
120. A. Kirchon, G. S. Day, Y. Fang, S. Banerjee, O. K. Ozdemir and H. C. Zhou, *iScience*, 2018, **5**, 30-37.
121. L. Qian and H. Zhang, *J. Chem. Tech. Biotech.*, 2011, **86**, 172-184.
122. L. Ma, A. Jin, Z. Xie and W. Lin, *Angew. Chem., Int. Ed.*, 2009, **48**, 9905-9908.
123. Q. Fu, L. Wen, L. Zhang, X. Chen, D. Pun, A. Ahmed, Y. Yang and H. Zhang, *ACS Appl. Mater. Interfaces*, 2017, **9**, 33979-33988.
124. E. J. Gosselin, G. R. Lorzing, B. A. Trump, C. M. Brown and E. D. Bloch, *Chem. Commun.*, 2018, **54**, 6392-6395.
125. Y. He, Z. Guo, S. Xiang, Z. Zhang, W. Zhou, F. R. Fronczek, S. Parkin, S. T. Hyde, M. O'Keeffe and B. Chen, *Inorg. Chem.*, 2013, **52**, 11580-11584.
126. L. Li, S. Tang, X. Lv, M. Jiang, C. Wang and X. Zhao, *New J. Chem.*, 2013, **37**.
127. H. Ma, S. Wang, H. Liu, F. Meng, W. Zheng and W. Gao, *CrystEngComm*, 2015, **17**, 1001-1004.
128. Y.-P. He, Y.-X. Tan and J. Zhang, *Inorg. Chem.*, 2012, **51**, 11232-11234.
129. Y. Kalinovskyy, N. J. Cooper, M. J. Main, S. J. Holder and B. A. Blight, *Dalton Trans*, 2017, **46**, 15704-15709.
130. E. J. Lee, J. Bae, K. M. Choi and N. C. Jeong, *ACS Appl Mater Interfaces*, 2019, **11**, 35155-35161.
131. F. Vermoortele, B. Bueken, G. Le Bars, B. Van de Voorde, M. Vandichel, K. Houthoofd, A. Vimont, M. Daturi, M. Waroquier, V. Van Speybroeck, C. Kirschhock and D. E. De Vos, *J. Am. Chem. Soc.*, 2013, **135**, 11465-11468.
132. Y. Feng, Q. Chen, M. Jiang and J. Yao, *Industrial & Engineering Chemistry Research*, 2019, **58**, 17646-17659.
133. D. Feng, Z.-Y. Gu, J.-R. Li, H.-L. Jiang, Z. Wei and H.-C. Zhou, *Angew. Chem., Int. Ed.*, 2012, **51**, 10307-10310.
134. J. E. Mondloch, W. Bury, D. Fairen-Jimenez, S. Kwon, E. J. DeMarco, M. H. Weston, A. A. Sarjeant, S. T. Nguyen, P. C. Stair, R. Q. Snurr, O. K. Farha and J. T. Hupp, *J. Am. Chem. Soc.*, 2013, **135**, 10294-10297.
135. P. Deria, J. Yu, T. Smith and R. P. Balaraman, *J. Am. Chem. Soc.*, 2017, **139**, 5973-5983.
136. T.-F. Liu, N. A. Vermeulen, A. J. Howarth, P. Li, A. A. Sarjeant, J. T. Hupp and O. K. Farha, *Eur. J. Inorg. Chem.*, 2016, **2016**, 4349-4352.
137. S. Kato, R. J. Drout and O. K. Farha, *Cell Rep. Phys. Sci.*, 2020, **1**, 100006.
138. X. S. Wu, X. L. Wang, F. L. Zhu, H. F. Bao, C. Qin and Z. M. Su, *Chem. Commun.*, 2018, **54**, 5474-5477.
139. C. R. Wade and M. Dincă, *Dalton Trans.*, 2012, **41**, 7931-7938.
140. T. Düren, Y.-S. Bae and R. Q. Snurr, *Chem. Soc. Rev.*, 2009, **38**, 1237-1247.
141. C. E. Wilmer, M. Leaf, C. Y. Lee, O. K. Farha, B. G. Hauser, J. T. Hupp and R. Q. Snurr, *Nat. Chem.*, 2012, **4**, 83-89.
142. P. G. Boyd, A. Chidambaram, E. García-Díez, C. P. Ireland, T. D. Daff, R. Bounds, A. Gładysiak, P. Schouwink, S. M. Moosavi, M. M. Maroto-Valer, J. A. Reimer, J. A. R. Navarro, T. K. Woo, S. Garcia, K. C. Stylianou and B. Smit, *Nature*, 2019, **576**, 253-256.
143. R. R. Maldonado, X. Zhang, S. Hanna, X. Gong, N. C. Gianneschi, J. T. Hupp and O. K. Farha, *Dalton Trans.*, 2020, **49**, 6553-6556.
144. L. Ma, J. M. Falkowski, C. Abney and W. Lin, *Nat. Chem.*, 2010, **2**, 838-846.
145. H. Jiang, W. Zhang, X. Kang, Z. Cao, X. Chen, Y. Liu and Y. Cui, *J. Am. Chem. Soc.*, 2020, 10.1021/jacs.0c00637.
146. H. Deng, S. Grunder, K. E. Cordova, C. Valente, H. Furukawa, M. Hmadeh, F. Gándara, A. C. Whalley, Z. Liu, S. Asahina, H. Kazumori, M. O'Keeffe, O. Terasaki, J. F. Stoddart and O. M. Yaghi, *Science*, 2012, **336**, 1018.
147. M. Eddaoudi, J. Kim, N. Rosi, D. Vodak, J. Wachter, M. Keeffe and O. M. Yaghi, *Science*, 2002, **295**, 469.
148. Q. Li, W. Zhang, O. Š. Miljanić, C.-H. Sue, Y.-L. Zhao, L. Liu, C. B. Knobler, J. F. Stoddart and O. M. Yaghi, *Science*, 2009, **325**, 855.
149. C. Liu, C. Zeng, T.-Y. Luo, A. D. Merg, R. Jin and N. L. Rosi, *J. Am. Chem. Soc.*, 2016, **138**, 12045-12048.
150. G. E. M. Schukraft, S. Ayala, B. L. Dick and S. M. Cohen, *Chem. Commun.*, 2017, **53**, 10684-10687.
151. Q. Yao, A. Bermejo Gómez, J. Su, V. Pascanu, Y. Yun, H. Zheng, H. Chen, L. Liu, H. N. Abdelhamid, B. Martín-Matute and X. Zou, *Chem. Mater.*, 2015, **27**, 5332-5339.
152. P. Guo, D. Dutta, A. G. Wong-Foy, D. W. Gidley and A. J. Matzger, *J. Am. Chem. Soc.*, 2015, **137**, 2651-2657.
153. P. Li, Q. Chen, T. C. Wang, N. A. Vermeulen, B. L. Mehdi, A. Dohnalkova, N. D. Browning, D. Shen, R. Anderson, D. A. Gómez-Gualdrón, F. M. Cetin, J. Jagiello, A. M. Asiri, J. F. Stoddart and O. K. Farha, *Chem*, 2018, **4**, 1022-1034.
154. N. L. Rosi, M. Eddaoudi, J. Kim, M. O'Keeffe and O. M. Yaghi, *Angew. Chem., Int. Ed.*, 2002, **41**, 284-287.
155. F. Nouar, J. F. Eubank, T. Bousquet, L. Wojtas, M. J. Zaworotko and M. Eddaoudi, *J. Am. Chem. Soc.*, 2008, **130**, 1833-1835.
156. Y. Yan, X. Lin, S. Yang, A. J. Blake, A. Dailly, N. R. Champness, P. Hubberstey and M. Schröder, *Chem. Commun.*, 2009, 10.1039/B900013E, 1025-1027.
157. D. Zhao, D. Yuan, D. Sun and H.-C. Zhou, *J. Am. Chem. Soc.*, 2009, **131**, 9186-9188.

158. J. F. Eubank, F. Nouar, R. Luebke, A. J. Cairns, L. Wojtas, M. Alkordi, T. Bousquet, M. R. Hight, J. Eckert, J. P. Embs, P. A. Georgiev and M. Eddaoudi, *Angew. Chem., Int. Ed.*, 2012, **51**, 10099-10103.
159. Y. Yan, M. Juríček, F.-X. Coudert, N. A. Vermeulen, S. Grunder, A. Dailly, W. Lewis, A. J. Blake, J. F. Stoddart and M. Schröder, *J. Am. Chem. Soc.*, 2016, **138**, 3371-3381.
160. O. K. Farha, C. D. Malliakas, M. G. Kanatzidis and J. T. Hupp, *J. Am. Chem. Soc.*, 2010, **132**, 950-952.
161. R. K. Deshpande, J. L. Minnaar and S. G. Telfer, *Angew. Chem., Int. Ed.*, 2010, **49**, 4598-4602.
162. Y.-Q. Lan, S.-L. Li, H.-L. Jiang and Q. Xu, *Chem.Eur. J.*, 2012, **18**, 8076-8083.
163. R. J. Marshall, C. T. Lennon, A. Tao, H. M. Senn, C. Wilson, D. Fairen-Jimenez and R. S. Forgan, *J. Mater. Chem. A*, 2018, **6**, 1181-1187.
164. T. K. Prasad and M. P. Suh, *Chem.Eur. J.*, 2012, **18**, 8673-8680.
165. P. Müller, F. M. Wisser, V. Bon, R. Grünker, I. Senkovska and S. Kaskel, *Chem. Mater.*, 2015, **27**, 2460-2467.
166. A. M. Bumstead, D. B. Cordes, D. M. Dawson, K. K. Chakarova, M. Y. Mihaylov, C. L. Hobday, T. Duren, K. I. Hadjiivanov, A. M. Z. Slawin, S. E. Ashbrook, R. R. R. Prasad and P. A. Wright, *Chem-Eur J*, 2018, **24**, 6115-6126.
167. D. Bara, C. Wilson, M. Mörtel, M. M. Khusniyarov, S. Ling, B. Slater, S. Sproules and R. S. Forgan, *J. Am. Chem. Soc.*, 2019, **141**, 8346-8357.
168. X. He, X.-P. Lu, Y.-Y. Tian, M.-X. Li, S. Zhu, F. Xing and R. E. Morris, *CrystEngComm*, 2013, **15**, 9437-9443.
169. Y. Wang, L. Cheng, K.-J. Wang, Z. Perry, W. Jia, R. Chen, Z.-L. Wang and J. Pang, *Inorg. Chem.*, 2019, **58**, 18-21.
170. H.-L. Jiang, Y. Tatsu, Z.-H. Lu and Q. Xu, *J. Am. Chem. Soc.*, 2010, **132**, 5586-5587.
171. J. Zhang, L. Wojtas, R. W. Larsen, M. Eddaoudi and M. J. Zaworotko, *J. Am. Chem. Soc.*, 2009, **131**, 17040-17041.
172. D. O'Nolan, D. G. Madden, A. Kumar, K.-J. Chen, T. Pham, K. A. Forrest, E. Patyk-Kazmierczak, Q.-Y. Yang, C. A. Murray, C. C. Tang, B. Space and M. J. Zaworotko, *Chem. Commun.*, 2018, **54**, 3488-3491.
173. R. Zhang, J.-H. Huang, D.-X. Meng, F.-Y. Ge, L.-F. Wang, Y.-K. Xu, X.-G. Liu, M.-M. Meng, Z.-Z. Lu, H.-G. Zheng and W. Huang, *Dalton Trans.*, 2020, **49**, 5618-5624.
174. R. Sanii, C. Hua, E. Patyk-Kaźmierczak and M. J. Zaworotko, *Chem. Commun.*, 2019, **55**, 1454-1457.
175. S. Bureekaew, H. Sato, R. Matsuda, Y. Kubota, R. Hirose, J. Kim, K. Kato, M. Takata and S. Kitagawa, *Angewandte Chemie*, 2010, **122**, 7826-7830.
176. B. D. McCarthy, T. Liseev, A. M. Beiler, K. L. Materna and S. Ott, *ACS Appl. Mater. Interfaces*, 2019, **11**, 38294-38302.
177. Y. Zhang, L. Wang, J. Hu, S. Duttwyler, X. Cui and H. Xing, *CrystEngComm*, 2020, **22**, 2649-2655.
178. A. Ferguson, L. Liu, S. J. Tapperwijn, D. Perl, F.-X. Coudert, S. Van Cleuvenbergen, T. Verbiest, M. A. van der Veen and S. G. Telfer, *Nat. Chem.*, 2016, **8**, 250.
179. B. Wang, X. L. Lv, D. Feng, L. H. Xie, J. Zhang, M. Li, Y. Xie, J. R. Li and H. C. Zhou, *J. Am. Chem. Soc.*, 2016, **138**, 6204-6216.
180. T. F. Liu, N. A. Vermeulen, A. J. Howarth, P. Li, A. A. Sarjeant, J. T. Hupp and O. K. Farha, *European Journal of Inorganic Chemistry*, 2016, 4349-4352.
181. O. Shekhah, H. Wang, M. Paradinas, C. Ocal, B. Schüpbach, A. Terfort, D. Zacher, R. A. Fischer and C. Wöll, *Nature Materials*, 2009, **8**, 481-484.
182. H. Furukawa, K. E. Cordova, M. O'Keeffe and O. M. Yaghi, *Science*, 2013, **341**, 1230444.
183. A. J. Howarth, Y. Liu, P. Li, Z. Li, T. C. Wang, J. T. Hupp and O. K. Farha, *Nat. Rev. Mater.*, 2016, **1**, 15018.
184. B. Rungtaweevoranit, C. S. Diercks, M. J. Kalmutzki and Omar M. Yaghi, *Faraday Discuss.*, 2017, **201**, 9-45.
185. N. Li, J. Xu, R. Feng, T.-L. Hu and X.-H. Bu, *Chem. Commun.*, 2016, **52**, 8501-8513.
186. J.-S. Qin, S. Yuan, C. Lollar, J. Pang, A. Alsalme and H.-C. Zhou, *Chem. Commun.*, 2018, **54**, 4231-4249.
187. C. Wang, X. Liu, N. Keser Demir, J. P. Chen and K. Li, *Chem. Soc. Rev.*, 2016, **45**, 5107-5134.
188. A. Corma, H. García and F. X. Llabrés i Xamena, *Chem. Rev.*, 2010, **110**, 4606-4655.
189. J. Liu, L. Chen, H. Cui, J. Zhang, L. Zhang and C.-Y. Su, *Chem. Soc. Rev.*, 2014, **43**, 6011-6061.
190. P. Li, Justin A. Modica, Ashlee J. Howarth, E. Vargas L, Peyman Z. Moghadam, Randall Q. Snurr, M. Mrksich, Joseph T. Hupp and Omar K. Farha, *Chem*, 2016, **1**, 154-169.
191. P. Li, S.-Y. Moon, M. A. Guelta, S. P. Harvey, J. T. Hupp and O. K. Farha, *J. Am. Chem. Soc.*, 2016, **138**, 8052-8055.
192. X. Liu, X. Wang and F. Kapteijn, *Chem. Rev.*, 2020, 10.1021/acs.chemrev.9b00746.
193. M. J. Kalmutzki, C. S. Diercks and O. M. Yaghi, *Adv. Mater.*, 2018, **30**, 1704304.
194. S. Yuan, L. Feng, K. Wang, J. Pang, M. Bosch, C. Lollar, Y. Sun, J. Qin, X. Yang, P. Zhang, Q. Wang, L. Zou, Y. Zhang, L. Zhang, Y. Fang, J. Li and H.-C. Zhou, *Adv. Mater.*, 2018, **30**, 1704303.
195. S. Biswas, M. Grzywa, H. P. Nayek, S. Dehnen, I. Senkovska, S. Kaskel and D. Volkmer, *Dalton Trans.*, 2009, 10.1039/B904280F, 6487-6495.
196. J. Teufel, H. Oh, M. Hirscher, M. Wahiduzzaman, L. Zhechkov, A. Kuc, T. Heine, D. Denysenko and D. Volkmer, *Adv. Mater.*, 2013, **25**, 635-639.
197. P.-Q. Liao, H. Chen, D.-D. Zhou, S.-Y. Liu, C.-T. He, Z. Rui, H. Ji, J.-P. Zhang and X.-M. Chen, *Energy & Environmental Science*, 2015, **8**, 1011-1016.
198. J.-P. Zhang, Y.-B. Zhang, J.-B. Lin and X.-M. Chen, *Chem. Rev.*, 2012, **112**, 1001-1033.
199. K. Wang, X.-L. Lv, D. Feng, J. Li, S. Chen, J. Sun, L. Song, Y. Xie, J.-R. Li and H.-C. Zhou, *J. Am. Chem. Soc.*, 2016, **138**, 914-919.
200. H. J. Choi, M. Dincă and J. R. Long, *J. Am. Chem. Soc.*, 2008, **130**, 7848-7850.
201. V. Colombo, S. Galli, H. J. Choi, G. D. Han, A. Maspero, G. Palmisano, N. Masciocchi and J. R. Long, *Chem. Sci.*, 2011, **2**, 1311-1319.
202. S. S. Y. Chui, S. M. F. Lo, J. P. H. Charmant, A. G. Orpen and I. D. Williams, *Science*, 1999, **283**, 1148.
203. T.-F. Liu, L. Zou, D. Feng, Y.-P. Chen, S. Fordham, X. Wang, Y. Liu and H.-C. Zhou, *J. Am. Chem. Soc.*, 2014, **136**, 7813-7816.
204. X. Lian, D. Feng, Y.-P. Chen, T.-F. Liu, X. Wang and H.-C. Zhou, *Chem. Sci.*, 2015, **6**, 7044-7048.
205. J. Park, D. Feng and H.-C. Zhou, *J. Am. Chem. Soc.*, 2015, **137**, 11801-11809.
206. S. M. Towsif Abtab, D. Alezi, P. M. Bhatt, A. Shkurenko, Y. Belmabkhout, H. Aggarwal, Ł. J. Weseliński, N. Alsadun, U. Samin, M. N. Hedhili and M. Eddaoudi, *Chem*, 2018, **4**, 94-105.
207. Z. Chen, P. Li, X. Zhang, P. Li, M. C. Wasson, T. Islamoglu, J. F. Stoddart and O. K. Farha, *J. Am. Chem. Soc.*, 2019, **141**, 2900-2905.

208. T. Wu, L. Shen, M. Luebbers, C. Hu, Q. Chen, Z. Ni and R. I. Masel, *Chem. Commun.*, 2010, **46**, 6120-6122.
209. J. Yang, A. Grzech, F. M. Mulder and T. J. Dingemans, *Chem. Commun.*, 2011, **47**, 5244-5246.
210. T.-H. Chen, I. Popov, O. Zenasni, O. Daugulis and O. Š. Miljanić, *Chem. Commun.*, 2013, **49**, 6846-6848.
211. H. Jasuja, N. C. Burtch, Y.-g. Huang, Y. Cai and K. S. Walton, *Langmuir*, 2013, **29**, 633-642.
212. H. Jasuja, Y.-g. Huang and K. S. Walton, *Langmuir*, 2012, **28**, 16874-16880.
213. M. Zhu, P. Hu, Z. Tong, Z. Zhao and Z. Zhao, *Chem. Eng. J.*, 2017, **313**, 1122-1131.
214. N. M. Padial, E. Quartapelle Procopio, C. Montoro, E. López, J. E. Oltra, V. Colombo, A. Maspero, N. Masciocchi, S. Galli, I. Senkovska, S. Kaskel, E. Barea and J. A. R. Navarro, *Angew. Chem., Int. Ed.*, 2013, **52**, 8290-8294.
215. H. He, Q. Sun, W. Gao, J. A. Perman, F. Sun, G. Zhu, B. Aguila, K. Forrest, B. Space and S. Ma, *Angew. Chem., Int. Ed.*, 2018, **57**, 4657-4662.
216. J. Lyu, X. Zhang, Z. Chen, R. Anderson, X. Wang, M. C. Wasson, P. Bai, X. Guo, T. Islamoglu, D. A. Gómez-Gualdrón and O. K. Farha, *ACS Appl. Mater. Interfaces*, 2019, **11**, 42179-42185.

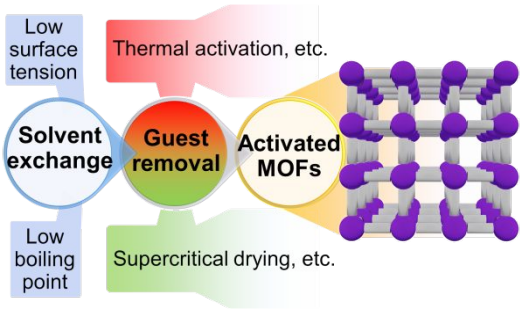

A historical overview of the activation and porosity of MOFs including strategies to design and preserve permanent porosity in MOFs.